Shibata et al. Molecular Brain 2010, 3:31
http://www.molecularbrain.com/content/3/1/31

Molecular Brain

RESEARCH Open Access

Sox10-Venus mice: a new tool for real-time labeling of neural crest lineage cells and oligodendrocytes

Shinsuke Shibata[1], Akimasa Yasuda[1,2], Francois Renault-Mihara[1,2], Satoshi Suyama[1], Hiroyuki Katoh[1,2,3], Takayoshi Inoue[4], Yukiko U Inoue[4], Narihito Nagoshi[1,2,3], Momoka Sato[1,2], Masaya Nakamura[2], Chihiro Akazawa[5], Hideyuki Okano[1*]

Abstract

Background: While several mouse strains have recently been developed for tracing neural crest or oligodendrocyte lineages, each strain has inherent limitations. The connection between human *SOX10* mutations and neural crest cell pathogenesis led us to focus on the *Sox10* gene, which is critical for neural crest development. We generated *Sox10*-Venus BAC transgenic mice to monitor Sox10 expression in both normal development and in pathological processes.

Results: Tissue fluorescence distinguished neural crest progeny cells and oligodendrocytes in the *Sox10*-Venus mouse embryo. Immunohistochemical analysis confirmed that Venus expression was restricted to cells expressing endogenous Sox10. Time-lapse imaging of various tissues in *Sox10*-Venus mice demonstrated that Venus expression could be visualized at the single-cell level *in vivo* due to the intense, focused Venus fluorescence. In the adult *Sox10*-Venus mouse, several types of mature and immature oligodendrocytes along with Schwann cells were clearly labeled with Venus, both before and after spinal cord injury.

Conclusions: In the newly-developed *Sox10*-Venus transgenic mouse, Venus fluorescence faithfully mirrors endogenous Sox10 expression and allows for *in vivo* imaging of live cells at the single-cell level. This *Sox10*-Venus mouse will thus be a useful tool for studying neural crest cells or oligodendrocytes, both in development and in pathological processes.

Background

The neural crest (NC) is a transient embryonic tissue. NC cells delaminate from the dorsal neural tube as it closes [1] and migrate to distinct locations, where they differentiate into various cell types, including neurons, glia, melanocytes, endocrine cells, and mesenchymal cells [2-5].

The Sox proteins belong to the HMG (high mobility group) domain of transcription factors [6,7]. Sox-E is the earliest marker of a subset of cells at the border of the neural plate that will give rise to NC-lineage cells [8]. Sox10, which is a member of the Sox-E family and shares high sequence homology with other Sox-E member transcription factors, regulates and coordinates diverse developmental processes such as organ development and cell survival and specification. Sox10 is highly expressed in the emerging NC and later in the developing glial cells of the peripheral nervous system (PNS) and central nervous system (CNS) [9,10]. Whether in mice or humans, Sox family protein deletions or mutations often result in developmental defects and congenital disease, and mutations of the human *SOX10* gene are associated with NC cell abnormalities [9,11-13].

Several transgenic mouse strains dedicated to tracing the NC lineage have already been developed, such as *Wnt1*-Cre [14], *Protein zero (P0)*-Cre [15], and *Ht-PA*-Cre [16] mice crossed with Cre-dependent reporter mice. The Cre recombinase expression was previously visualized by *LacZ*, a β-galactosidase reporter gene inserted in the ROSA26 locus, that is expressed only

* Correspondence: hidokano@sc.itc.keio.ac.jp
[1]Department of Physiology, Keio University School of Medicine, Shinjuku-ku, Tokyo 160-8582, Japan
Full list of author information is available at the end of the article

after the loxP-flanked intervening sequence is excised by Cre [17]. Once a specific promoter is activated, the cell is indelibly tagged with β-galactosidase. This kind of transgenic mouse is useful for monitoring the transient activation of various promoters, including the NC-specific promoter. Recently, mouse strains expressing a fluorescence-based reporter upon Cre-mediated conditional gene deletion have been developed for prospective cell sorting or direct observation without fixation [18]; the CAG-CAT-EGFP reporter transgenic mouse strain expresses enhanced green fluorescent protein (EGFP) when the loxP-flanked CAT gene located between the modified chicken β-actin promoter (CAG promoter) and the EGFP gene [18] is excised with Cre. In previous studies, we have used mice that enable Cre/loxP-mediated cell labeling with *LacZ* or EGFP to analyze the NC lineage and to trace NC cells after their migration and differentiation [5,19-21].

However, for specific gene regulation analysis, transgenic or knock-in mouse lines that express a specific gene profile *in vivo* are more useful, because the reporter gene is expressed only while the specific promoter or enhancer is active, and ceases when the promoter becomes inactive. Reporter mice have recently been developed to evaluate cell-type specification and maturation in the oligodendroglial lineage; these are the 2'-3'-cyclic nucleotide 3'-phosphodiesterase (*CNP*)-EGFP and myelin proteolipid protein (*PLP*)-EGFP transgenic mouse lines [22,23]. The *CNP*-EGFP transgenic mouse, in which the CNP promoter controls EGFP expression, has been used for the prospective identification of live oligodendroglial cells both *in vivo* and *in vitro* [23]. The *PLP*-EGFP transgenic mouse, in which EGFP expression is driven by the mouse *PLP* gene promoter, has also been developed for investigating oligodendrocyte lineage cells without fixation and immunostaining [22].

Sox10 expression is closely related to NC-lineage cells. The *Sox10*$^{LacZ/+}$ [24], *Sox10*-rtTA [25], and *Sox10*-Cre [26] mouse lines have all been reported to label NC cells and oligodendrocytes. *Sox10*$^{LacZ/+}$ [24], a mutant mouse targeting *Sox10*, was generated by replacing the open reading frame of *Sox10* with *lacZ* sequences. The *Sox10*-$^{LacZ/+}$ mutation causes haploinsufficiency, in which even heterozygous pups have the phenotype found in mice with a spontaneous mutation in the *Sox10* allele. Although *LacZ* expression in this knock-in strain faithfully reflects the endogenous Sox10 expression, it is difficult to observe normal developmental behavior in the labeled cells because of the abnormal and pathological condition of the *Sox10*$^{LacZ/LacZ}$ homozygous mice [24]. Another unique reporter strain is the *Sox10*-rtTA knock-in mouse [25], in which a variant of the reverse tetracycline-controlled transactivator (rtTA) is inserted into the genomic *Sox10* locus, and the mice are crossed with the doxycycline-dependent *LacZ* reporter line. This strain correctly recapitulates endogenous Sox10 expression in the NC and its derivatives, and also in oligodendrocytes. This inducible transgenic system is limited in its range of analysis, because the reporter gene expression is temporary and requires X-gal staining [25]. The *Sox10*-Cre transgenic mouse strain, designated as the S4F:Cre mouse, when crossed with the reporter line strain Rosa-*LacZ*, identifies cells expressing Sox10, including NC-derived cells, oligodendrocytes, and cells in the ventral neural tube [26]. These strains are powerful tools for tracing the progeny of Sox10-expressing cells in analyses of NC cell migration and oligodendroglial differentiation. However, permanent reporter gene expression does not permit the real-time analysis of Sox10 expression. To overcome these limitations, we generated a new *Sox10*-Venus transgenic mouse, and confirmed that it enables the normal behavior of Sox10-expressing cells to be observed *in vivo*.

Results

Sox10-Venus BAC transgenic mouse generation

To examine the Sox10 expression profile *in vivo*, we took advantage of the bacterial artificial chromosome (BAC) transgenic strategy where entire regulatory machinery for a given gene expression might be covered with a single BAC clone. In short, we modified a 225.6 kb-sized BAC clone *RP24-85O14* by means of homologous recombination to harbor the coding sequence of the fluorescent Venus protein [27] in-frame to the *Sox10* translation initiation codon (ATG) that locates at the middle portion of the clone. This construct yielded seven BAC transgenic founders expressing Venus and we hereafter analyzed the complete expression profile in a particular transgenic founder with the brightest illumination.

First, we evaluated the distribution of Venus fluorescence at each developmental stage of the *Sox10*-Venus mouse embryo. Venus fluorescence in classical NC lineage tissues was directly visible from outside the embryo by using an epifluorescence microscope and a UV light. At embryonic day 11.5 (E11.5 d), Venus green fluorescence was particularly intense in the dorsal root ganglia (DRG) and the trigeminal ganglia (cranial nerve V) (Figure 1A). We observed that Venus fluorescence was not limited to classical NC lineage tissue, but was also observed in non-NC tissues, including the otic vesicle. This is consistent with previous studies in which *in situ* hybridization revealed endogenous Sox10 expression in otic vesicle cells [28,29], which are the primitive state of the vestibulocochlear nucleus (cranial nerve VIII). In the facial area of the E11.5 d embryo, aggregated green cells were observed among scattered Venus-positive cells (Figure 1B). The intensity and resolution of the Venus fluorescence allowed

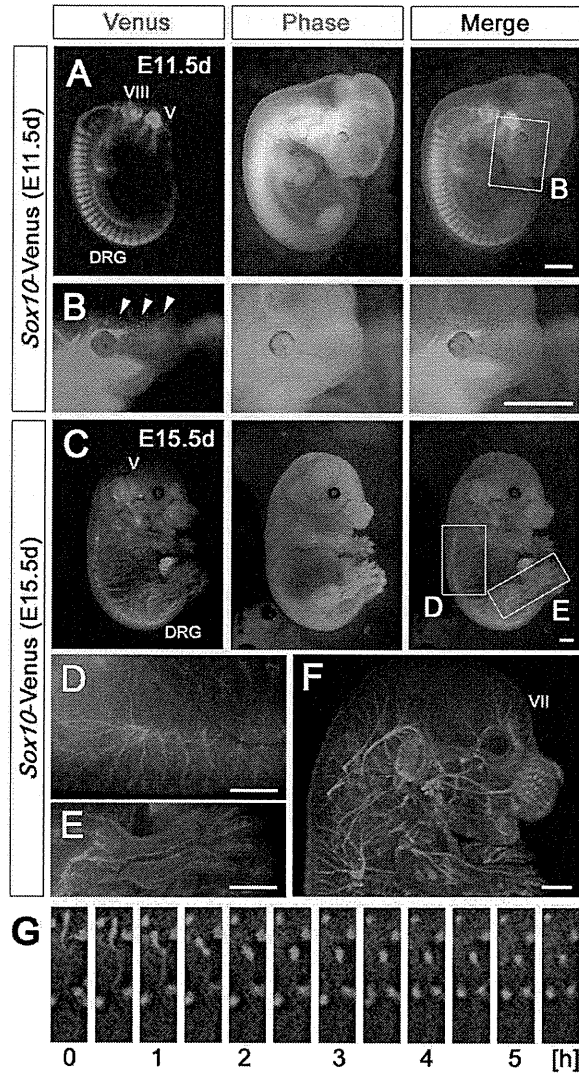

Figure 1 The novel *Sox10*-Venus transgenic mouse strain. The *Sox10*-Venus BAC transgenic mouse strain was generated to investigate the Sox10 expression profile *in vivo*. (A) Venus could be detected in NC lineage tissues, including the DRG and trigeminal ganglia, in E11.5 d mice. Sox10$^+$ cells that were not NC-derived, including cells in the otic vesicle, could also be visualized with Venus. (B) High-intensity fluorescence enabled us to observe a migration stream at the single-cell level, from outside the embryo. (C) At E15.5 d, deep-tissue Venus fluorescence decreased. At this age, migrating Venus$^+$ cells and the network formation of Venus$^+$ cells in the superficial skin layer could be traced. (D) The posterior branches of the spinal nerve were clearly visualized with Venus$^+$ Schwann cells, along with peripheral nerve fibers. (E) In the hind limb, the peripheral nerve and vascular network formations were clearly outlined. (F) The peripheral neural network mainly derived from cranial nerve VII could be visualized with three-dimensional reconstruction with an Olympus MVX-CSU microscope. (G) Time-lapse imaging of the front facial area of embryonic *Sox10*-Venus mice clearly showed individual Venus$^+$ cell movement (also shown in movies in Additional Files 2 and 3). (B) and (D, E) are high-magnification images of the indicated areas in Figures (A) and (C), respectively. Cranial nerves V, trigeminal nerve; VII, facial nerve; VIII, vestibulocochlear nerve, Scale bars; (A-F) 1.0 mm.

us to observe single cells in a pattern suggestive of the NC cell rostral migration process (arrowheads in Figure 1B). As development proceeded from E11.5 d to E15.5 d, Venus fluorescence from the DRGs and nuclei of the cranial nerves located in deep tissues gradually decreased, due to the thickening dermal layer (Figure 1A, C, and Additional file 1A - 1C). However, migrating Venus$^+$ cells in the superficial layer of the embryonic skin were now detectable from outside the body. Venus fluorescence was observed in the Schwann cells of the neural network stemming from the spinal nerve's posterior branches, and in peripheral sensory nerve fibers (Figure 1D). In the hind limb, the peripheral nerve network and the adjacent vascular network were visible (Figure 1E). Three-dimensional reconstructions of the peripheral nerve fibers displayed the entire neural network in the craniofacial area, which

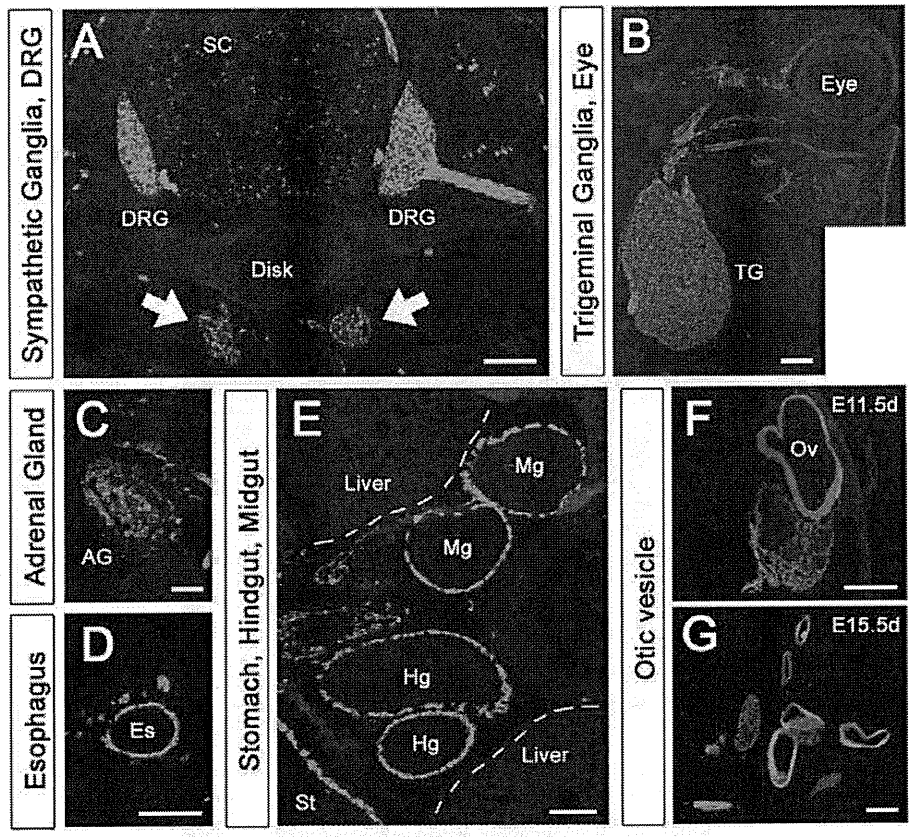

Figure 2 Venus expression in neural crest lineage tissues and in otic vesicle observed without immunostaining. The distribution of Venus$^+$ cells in *Sox10*-Venus mice was evaluated in embryonic-stage cryosections. Venus fluorescence was directly observed without immunostaining. (A) On the thoracic region of an E15.5 d axial section, Venus$^+$ cells were localized to the DRG and its central and peripheral branches. In the spinal cord, Venus$^+$ cells were broadly localized to both the gray matter and the white matter. Venus$^+$ sympathetic ganglion cells were also found at the ventral side of the vertebral body (arrows). (B) In an E15.5 d horizontal section of the cranial area, Venus$^+$ cells concentrated and formed the trigeminal ganglia (the nucleus of the V cranial nerve) and its first branch, the ocular nerve, also visualized by Venus. (C) Venus$^+$ cells were randomly localized in the E15.5 d adrenal gland. (D) NC-derived enteric ganglion cells were seen originating from the XII cranial nerve (Nervous Vargus) and migrating in an oral to anal direction in the alimentary tract. (D-E) On the lumbar level axial section, Venus$^+$ cells were captured in the esophagus, stomach, midgut, and hindgut in the stream of their migration. (F-G) The primary structure of the inner ear, designated as the otic vesicle, also expresses Venus in the embryonic period. The otic vesicle is not NC-derived, but expresses Sox10. SC, spinal cord; TG, trigeminal ganglia; AG, adrenal gland; Es, esophagus; St, stomach; Hg, hindgut; Mg, midgut; Ov, otic vesicle. Scale bars (A-C, E) 100 μm, (D, F-G) 50 μm.

was mainly derived from the branches of the facial nerve (cranial nerve VII) (Figure 1F).

Observing the behavior of individual *Sox10*-Venus cells

The intensity and resolution of the Venus fluorescence in the new *Sox10*-Venus mice led us to evaluate whether it was possible to monitor the behavior of individual cells. Time-lapse imaging *ex-vivo* in skin explants from E14.5 d *Sox10*-Venus embryos was first performed using an epifluorescence microscope. Within this experimental setup, it was easy to detect and follow the movements of single cells (Figure 1G and the movie in Additional File 2). As Sox10 is expressed in deep tissues during the early stages of development, we next examined whether it would be possible to observe Venus fluorescence in whole *Sox10*-Venus embryos. Whole embryos at E10.5 d were observed using a confocal microscope, and followed over time. Time-lapse imaging of the front facial area allowed us to monitor the migration of several Venus$^+$ cells within the embryo over a duration of several hours. We were also able to observe the shape dynamics of individual migrating cells (movie in Additional File 3).

Venus fluorescence in frozen sections of *Sox10*-Venus mice

To confirm the Venus$^+$ cell distribution, we prepared cryosections of *Sox10*-Venus mice from each embryonic stage and observed the Venus fluorescence directly, without any antibody staining or enhancement procedure

(Figure 2). In axial sections of the thoracic region of E15.5 d mouse embryos, Venus fluorescence was intense in the DRG and its proximal and peripheral branches (Figure 2A). Venus$^+$ cells were diffusely present throughout the spinal cord. Some ganglion cells were positive for Venus (Figure 2A, arrows) in the sympathetic ganglia located at the ventral side of the vertebral disc. In horizontal cranial sections from E15.5 d *Sox10*-Venus embryos, large numbers of Venus$^+$ cells accumulated to form the trigeminal ganglia (cranial nerve V) (Figure 2B). Venus was highly expressed in the ocular nerve, which is the first branch of the trigeminal nerve. Venus$^+$ cells were randomly distributed in the E15.5 d adrenal gland, most likely due to the incomplete column structure formation at this stage (Figure 2C). In the alimentary tract, Venus$^+$ enteric ganglion cells originating from the vagal nerve (cranial nerve XII) were found migrating in a rostrocaudal direction through the esophagus, stomach, midgut, and hindgut (Figure 2D and 2E). All of these tissues are well-known NC derivatives, demonstrating that the Venus fluorescence observed in the *Sox10*-Venus mice is consistent with known NC cell localization and differentiation [1-3,5]. In the otic vesicle, which is the primary structure of the inner ear nerve, cells continuously expressed Venus throughout the embryonic period (Figure 2F and 2G). The otic vesicle is not a NC derivative, but Sox10 protein expression in otic vesicle cells during the embryonic stage has been reported [28,29].

Cell type evaluation of the Venus$^+$ cells in *Sox10*-Venus mice

To verify that the Venus expression correctly reflects the endogenous expression of the Sox10 protein *in vivo*, we performed immunohistochemistry of E11.5 d to postnatal 1-week-old (P1 w) whole mouse frozen sections. Without exception, in all the tissues and stages examined, all the Sox10-positive cells expressed Venus. In addition to Sox10 immunostaining, we also examined cell-type-specific markers in NC-derived and Sox10$^+$ tissues. The enteric ganglion cells in the alimentary tract stained with PGP9.5 antibodies. In the esophagus, stomach, midgut, and hindgut, most of the migrated enteric ganglion cells were positive for Venus at E15.5 d (Figure 3A). In the E15.5 d adrenal gland stained for tyrosine hydroxylase (TH), a marker for catecholaminergic cells, TH-positive endocrine cells were positive for Venus (Figure 3B). In the early embryonic (E11.5 d) DRG, all Hu-positive sensory neurons were co-labeled with Sox10 and Venus (Figure 3C). These observations confirmed that *Sox10*-Venus is a useful reporter strain, in which Venus expression faithfully reflects the endogenous Sox10 *in vivo* expression.

Loss of Venus-fluorescence correlates with the shutdown of endogenous Sox10 expression

To evaluate the on/off switching of reporter gene activity in *Sox10*-Venus mice, we verified the Sox10 expression with immunohistochemistry, and examined its correlation with Venus fluorescence. At the late embryonic stage of E15.5 d, the loss of Sox10 expression in Hu-positive DRG neurons coincided with a dramatic decrease in Venus fluorescence, compared to the early embryonic stage (Figure 3C and 3D). A similar phenomenon was observed in embryonic sympathetic ganglia: most of the TH$^+$ neurons were Venus$^+$ in the early embryonic stage, while TH$^+$ neurons in the late embryonic stage lost both Venus and Sox10 expression (Figure 3E and 3F).

The prompt on/off switching of reporter gene activity is an important characteristic of this transgenic mouse strain. In mice in which the NC lineage is labeled, such as the *Wnt1*-Cre/CAG-CAT-EGFP double transgenic mouse, NC progeny expressing Cre are indelibly labeled with the reporter gene. At the late embryonic stage of E15.5 d, neurons in the DRG and sympathetic ganglia of *Wnt1*-Cre/CAG-CAT-EGFP mice were still labeled with EGFP fluorescence even though endogenous Sox10 expression had already diminished (Additional file 4). In contrast, the sensitive on-off switching of the Venus-fluorescent reporting makes the *Sox10*-Venus mouse an accurate, real-time reporter strain.

Identification of Venus$^+$ cells in the intact embryonic spinal cord

Previous reports have suggested that Sox10 is expressed in oligodendrocyte progenitor cells (OPCs) and mature oligodendrocytes [24-26]. We examined the identity of the Venus$^+$ cells observed in the ventral region of the intact embryonic spinal cord of *Sox10*-Venus mice by immunohistochemistry. The Venus$^+$ cells were negative for the pan-neuronal marker Hu (Figure 4A), but positive for the oligodendroglial-lineage markers GSTπ and Olig2 (Figure 4B and 4C). Therefore, in the spinal cord of the embryonic *Sox10*-Venus mouse, Venus labels oligodendroglial-lineage cells without distinction as to their degree of maturation.

Venus$^+$ cells in the intact and injured spinal cords of adult *Sox10*-Venus mice

To examine the phenotype of Venus$^+$ cells in intact and injured spinal cords of *Sox10*-Venus mice, we first observed changes in the Venus$^+$ cells over time (Figure 5A - C). After spinal cord injury (SCI), there was a sharp drop in the number of Venus$^+$ cells, followed by a gradual accumulation around the lesion epicenter at later stages after the injury.

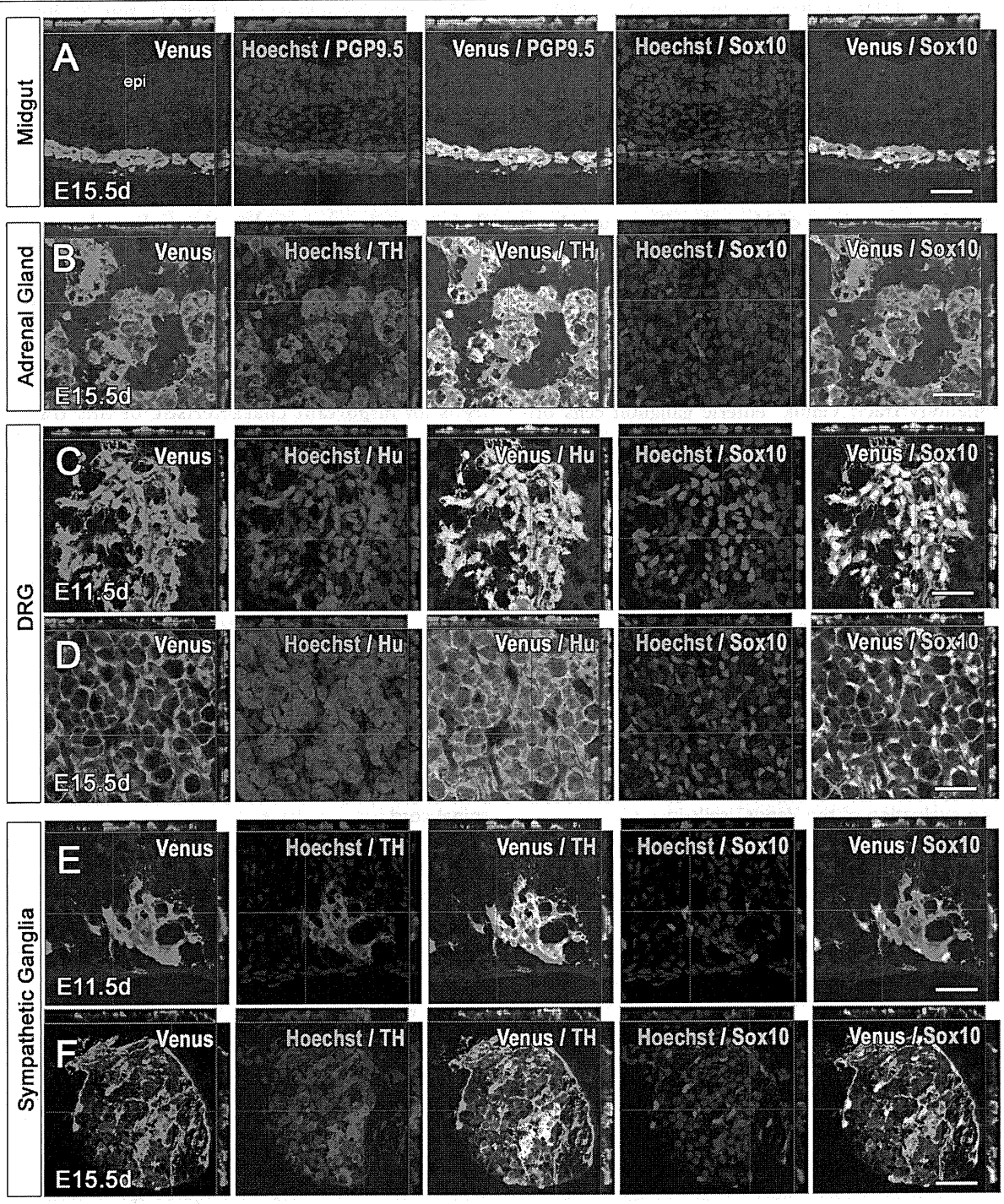

Figure 3 Venus expression faithfully reflects endogenous Sox10 expression. Immunohistochemistry was used to confirm the *in vivo* co-localization of Venus with specific cell-type markers in *Sox10*-Venus mice. (A-F) All Sox10-positive cells were also positive for Venus; no ectopic Venus expression was detected in an entire series of sections. (A) In the E15.5 d alimentary tract, PGP9.5-positive enteric ganglion cells were also positive for Venus. (B) TH-positive endocrine cells in the E15.5 d adrenal gland were invariably positive for Venus. (C-D) While all Hu-positive early embryonic DRG neurons expressed endogenous Sox10 and Venus protein at E11.5 d, mature DRG neurons lost the Sox10 and Venus expression simultaneously at E15.5 d, and $Sox10^+$ satellite cells became positive for Venus. (E-F) In the embryonic sympathetic ganglia, all the TH^+ neurons were also $Venus^+$ at E11.5 d, whereas TH^+/$Venus^-$ cells appeared at E15.5 d. Hu^+, terminally differentiated neuron; $PGP9.5^+$, enteric ganglion cell; TH^+, adrenal gland endocrine cells and sympathetic ganglion neurons; epi, epithelium. Scale bars (A-F) 50 μm.

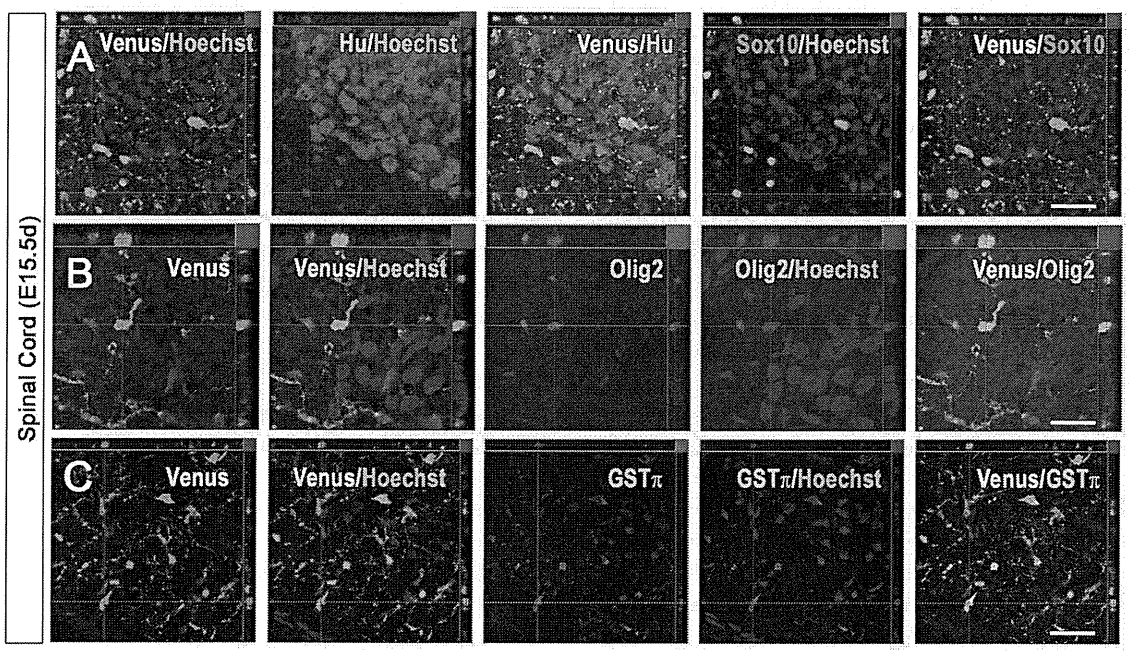

Figure 4 *Sox10*-Venus$^+$ cells in the intact embryonic spinal cord. Immunohistochemical analysis of Venus$^+$ cells in the intact embryonic spinal cord of *Sox10*-Venus mice. (A) Venus fluorescence did not colocalize with the pan-neuronal marker Hu in the ventral area of *Sox10*-Venus mice. (B-C) These Venus$^+$ cells expressed the oligodendroglial lineage markers GSTπ and Olig2, showing that the Venus$^+$ cells were OPCs and mature oligodendrocytes. Scale bars; (A-C) 50 μm.

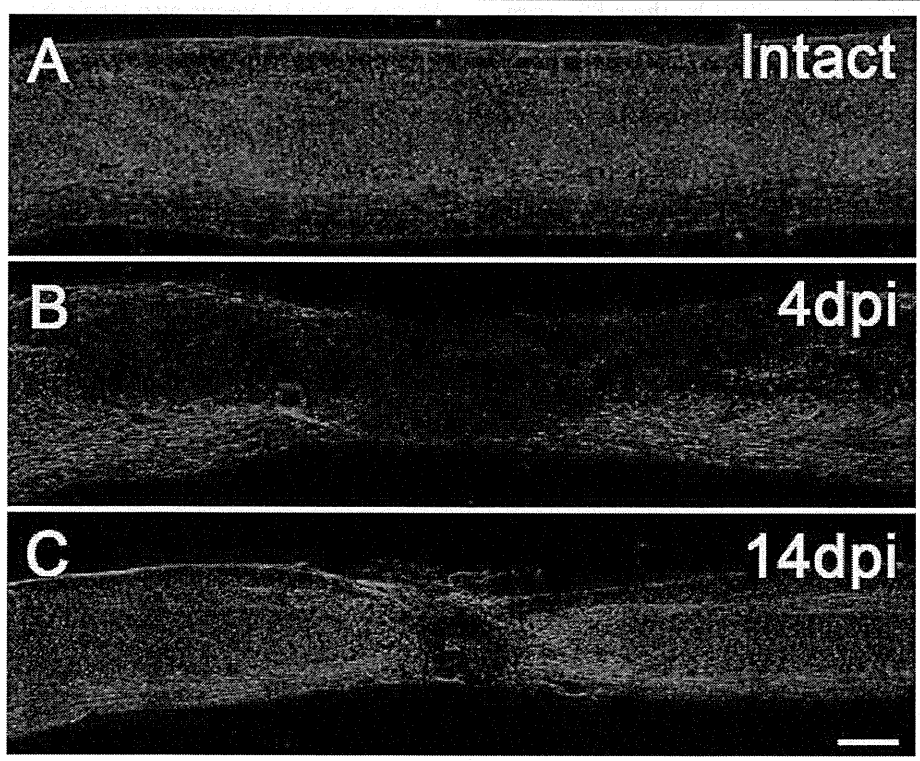

Figure 5 *Sox10*-Venus$^+$ cells actively accumulate at the spinal cord injury site. Venus fluorescence illuminated the behavior of *Sox10*-expressing cells after a spinal cord injury. (A) In an intact adult mouse spinal cord, Venus$^+$ cells were clearly visible in both in the gray and the white matter. (B) In the acute phase of contusive spinal cord injury (4 dpi; days-post-injury), Venus$^+$ cells were absent from the lesion site. (C) In the subacute phase (14 dpi), numerous Venus$^+$ cells were present around the lesion and delineated the lesion epicenter. Scale bars (A-C) 500 μm.

Next, we identified the Venus$^+$ cells in intact and injured spinal cords by immunostaining with various cell markers (Figure 6A - H). In the intact spinal cord, Venus$^+$ cells were easily visualized in both the gray and white matter (Figure 5A), and were mostly positive for GSTπ (Figure 6A). After contusive SCI, Sox10-expressing cells disappeared from the lesion epicenter (Figure 5B). In the acute phase of SCI (4 days-post-injury; 4 dpi), cells positive for NG2 and Venus appeared in the residual white matter (Figure 6B). Although NG2 is also known to stain reactive astrocytes and macrophages [30], the Venus$^+$ cells observed in the injured spinal cord were negative for GFAP (Figure 6D) and CD11b (Figure 6E), indicating that they were Sox10-expressing oligodendrocytes. We also observed Venus$^+$ cells that were positive for PDGFRα, an OPC marker (Figure 6C), suggesting that OPCs also expressed Sox10 in the injured spinal cord.

In the later subacute phase of SCI (14 dpi), numerous Venus$^+$ cells were found in the epicenter and around the lesion site (Figure 5C). Immunohistochemistry revealed that many of the Venus$^+$ cells were positive for S100β, a marker of the Schwann cell lineage, confirming Schwann cell involvement after SCI (Figure 6F). Some of the Venus$^+$ cells had bipolar processes and were positive for p75, suggesting that they were immature Schwann cells (Figure 6G), while a few Venus$^+$ mature Schwann cells were also identified by their P0 expression (Figure 6H). The observation that both immature and mature Schwann cells were Venus$^+$ in the injured spinal cord is consistent with the Schwann cell lineage deriving from the NC.

Comparison of the *Sox10*-Venus strain with other NC reporter mouse strains

The data from several NC reporter mouse lines, such as *Sox10*(S4F)-Cre, *P0*-Cre, *Wnt1*-Cre, and *Ht-Pa*-Cre [5,14,16,26,31,32], have already been published. To compare this body of data to the observations gained from the *Sox10*-Venus mouse, the embryonic expression patterns of various NC-derived tissues are summarized for each strain in Table 1. At the early embryonic period (E11.5 d - E12.5 d), the reporter gene activity of all the mouse strains was quite similar. All the strains demonstrated reporter gene activity in numerous NC-lineage tissues, including the DRG, sympathetic ganglia, melanoblasts, enteric nervous system, superior/jugular ganglion, aorta, and craniofacial mesenchyme. All the strains also showed reporter expression in the otic vesicle, which does not originate from the NC.

Regarding the differences in these reporter strains, CNS myelinating glial cells were not labeled in the *P0*-Cre, *Wnt1*-Cre, and *Ht-Pa*-Cre strains; they were only labeled in the *Sox10*-related strains *Sox10*-Venus and *Sox10* (S4F)-Cre. In the brain and spinal cord, the labeling of oligodendroglial cells and OPCs in the *Sox10*-Venus and *Sox10*-Cre mice reflected the endogenous Sox10 expression in these cells, since they are not derived from the NC. The peripheral nerve network in developing limbs consists of nerve fibers and their associated Schwann cells, which are both derived from the NC. Although the *LacZ* expression in the developing limb was ambiguous in the *Sox10*(S4F)-Cre/Rosa-*LacZ* mouse [26], the Venus fluorescence observed in the same region with the *Sox10*-Venus mouse clearly originated from the Schwann cells (Figure 1E).

Discussion

In this study, we developed and characterized the *Sox10*-Venus BAC transgenic mouse. Analysis of the early embryonic stages showed that not only NC lineage cells, but also oligodendroglial cells were clearly labeled with high-intensity Venus fluorescence (Figure 1 and 2). Compared to other published transgenic and knock-in reporter mouse strains, the *Sox10*-Venus mouse has advantages that make it invaluable for future studies.

The mice with NC-lineage tracing *Wnt1*-Cre, *P0*-Cre, and *Ht-PA*-Cre, crossed with those with Cre/loxP-mediated cell labeling, Rosa-*LacZ* and CAG-CAT-EGFP, can be used only for analyzing cell lineage or migration, because the target cells are irreversibly labeled [5,14-20]. Although *Sox10*-Venus also labels NC-lineage cells, the fast on/off switching of Venus fluorescence is tightly correlated with endogenous Sox10 expression. Similarly, the reporter gene activity in *CNP*-EGFP and *PLP*-EGFP mice, which are transgenic mice that label oligodendroglial-lineage cells, truly reflects the *in vivo* expression of specific genes driven by specific promoters or enhancers. The transgenic system of the *Sox10*-Venus mouse is quite similar to these; however, the Venus fluorescence is brighter and more intense than EGFP fluorescence.

Although reporter gene activity occurs in NC cells and oligodendrocytes in all *Sox10* reporter mouse lines, i.e., *Sox10*$^{LacZ/+}$, *Sox10*-rtTA, *Sox10*-Cre strains [24-26], and the new *Sox10*-Venus strain, each line has advantages and disadvantages. *LacZ* knock-in *Sox10*$^{LacZ/+}$ heterozygous pups are prone to spontaneous mutation phenotypes due to haploinsufficiency. Also, to observing the *LacZ* expression in *Sox10*$^{LacZ/+}$ mice requires additional visualization procedures, making live cell imaging difficult. The *Sox10*-rtTA knock-in crossed with the inducible TRE-*LacZ* transgenic is unique, but the reporter expression is transient and does not fluoresce, making it difficult to observe directly. The *Sox10*-Cre/CAG-CAT-EGFP double transgenic mouse traces both NC and oligodendrocyte progeny, since it reports past as well as ongoing Sox10 expression. With this double transgenic mouse, it is possible to carry out cell sorting or live imaging.

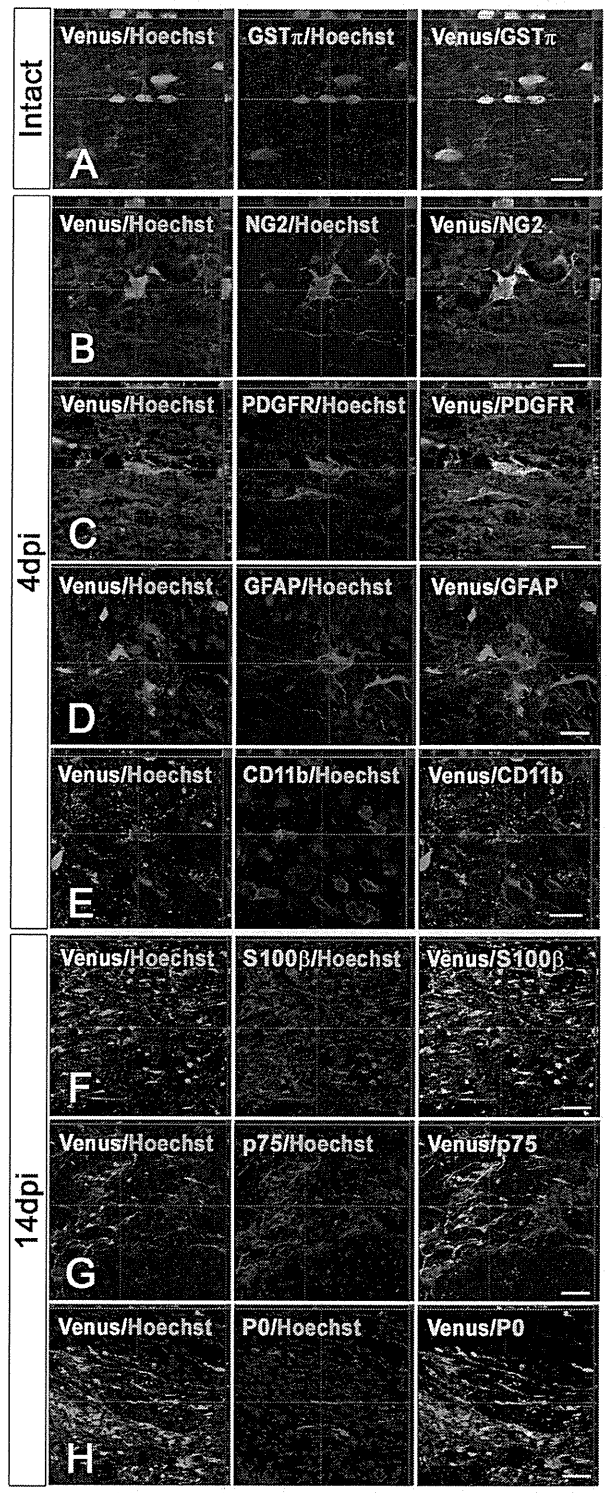

Figure 6 Immunohistochemical analysis of *Sox10*-Venus$^+$ cells after spinal cord injury. (A-E) OPCs and mature oligodendrocytes were Venus$^+$ in the intact and injured spinal cord of *Sox10*-Venus mice. (A) Most Venus$^+$ cells were positive for GSTπ in the intact spinal cord. (B) In the acute phase (4 dpi), NG2$^+$ cells increased in the residual white matter in response to the SCI. Some of the NG2$^+$ cells also expressed Venus. (C-E) In the acute phase, Venus$^+$ oligodendroglial cells were also positive for PDGFRα (C), but were negative for GFAP (D) and CD11b (E). (F) In the subacute phase of the SCI (14 dpi), S100β$^+$ cells were also present around the lesion site, and expressed Venus. (G) Some of the Venus$^+$ cells were positive for p75, suggesting that they were immature Schwann cells with bipolar processes. (H) A small number of Venus$^+$ cells were mature Schwann cells, as assessed by Protein Zero expression. Scale bars; (A-E) 20 μm, (F-H) 50 μm.

Table 1 Comparison of reporter expression in *Sox10*-Venus and various other mice with NC lineage-labeling

Tissues	*Sox10*-Venus	*Sox10*-Cre	*P0*-Cre	*Wnt1*-Cre	*Ht-Pa*-Cre
Dorsal root ganglia	+	+	+	+	+
Sympathetic ganglia	+	+	+	+	+
Melanoblasts	+	+	+	+	+
Enteric nervous system	+	+	+	+	+
Superior/jugular ganglion	+	+	+	+	+
Aortae	+	+	+	+	+
Craniofacial mesenchyme	+	+	+	+	+
Otic vessicle	+	+	+	+	+
Oligodendroglia	+	+	-	-	-
Ventral neural tube	+	+	-	-	-
Developing limb	+	+	-	-	-

Reporter gene expression patterns at the embryonic stage are compared in various mice developed to trace neural crest derivatives: *Sox10*-Venus, *Sox10*(S4F)-Cre [26], *P0*-Cre [5,15], *Wnt1*-Cre [14,16,26,31,32], and *Ht-Pa*-Cre [16,26]. All these lines have similar labeling patterns in both NC-lineage tissues (DRG, sympathetic ganglia, melanoblasts, enteric nervous system, superior/jugular ganglion, aorta, craniofacial mesenchyme) and in tissues not in the NC lineage (otic vesicle, oligodendroglial cells, and OPCs). In the developing limbs of *Sox10*-Venus and *Sox10*-Cre mice, which reflect the endogenous Sox10 expression profile, the reporter fluorescence clearly labeled oligodendroglial cells and the peripheral nervous network. Immunohistochemistry did not detect any ectopic reporter gene expression in any tissues from the embryonic *Sox10*-Venus mice.

The *Sox10*-Venus strain overcomes most of the disadvantages of the above-mentioned *Sox10* reporter mouse lines. In this mouse, the intense Venus fluorescence can be directly observed from outside the embryo, without staining or enhancement procedures (Figure 1, 2, and movies in Additional Files 2 and 3). Venus expression faithfully reflects real-time endogenous Sox10 expression, with prompt on/off switching (Figure 3). Although the choice of strain obviously depends on the purpose of the study, we believe that the *Sox10*-Venus mouse is the most appropriate reporter line for numerous fields of research.

Although *in vivo* time-lapse imaging of oligodendroglial cell migration (including OPCs) has recently been reported, it has only been conducted in zebrafish [33,34]. Accurate time-lapse imaging has been difficult to conduct in mice until now. There are several issues that need to be considered in such studies. For instance, (1) Is the *normal* and *natural* behavior of the cells or tissues of interest being observed? In some cases, the invasive procedures required to complete the imaging, including surgical incision, tissue-slice culture, electroporation, dye injection, and virus infection, may affect the tissues observed. (2) To what degree does the transgenic manipulation affect the phenotype? In $Sox10^{LacZ/+}$ mice, the resulting phenotype, coupled with haploinsufficiency, complicates analysis of the area of interest. Our analysis of the *Sox10*-Venus transgenic line demonstrates that it has neither developmental defects nor ectopic Venus expression. Thus, the *Sox10*-Venus strain appears to be a useful tool for investigating normal developmental processes via live cell monitoring, using directly observed fluorescence without invasive intervention procedures (Figure 1G, movies in Additional Files 2 and 3).

Sox10 is a well-known marker of neural crest stem cells (NCSCs), along with *slug, snail,* and *p75* [35,36]. There have been numerous reports recently of NCSCs surviving in a wide range of tissues through the entire lifespan of the animal, suggesting that NCSCs may have the potential to support the regeneration and recovery of damaged tissues. The Venus fluorescence in *Sox10*-Venus mice will make it possible to prospectively sort $Venus^+$ cells by flow-cytometry and collect an enriched population of NCSCs. Since NCSCs are located in easily accessible peripheral tissues such as the skin and bone marrow, NCSCs have been receiving increasing attention for future clinical applications in cell transplantation therapy, because the feasibility of autologous transplantation is anticipated [37-39]. Autologous cell transplantation therapy avoids the immunological and ethical concerns related to the use of embryonic stem cells. We hope that the *Sox10*-Venus strain will prove to be a powerful tool for enhancing the progress of NCSC research.

The mouse is an excellent model system for studying human disease progression and pathogenesis. We demonstrated the usefulness of our new reporter mouse strain *Sox10*-Venus for monitoring processes occurring after a traumatic disorder (Figure 5 and 6), and crossing it with mutant mouse lines may provide insight into the processes behind numerous developmental defects. As with the analysis conducted in CNP-EGFP mice to study the behavior of oligodendroglial cells in SCI [30], *Sox10*-Venus mice have potential applications not only for oligodendrocyte research, but also for all $Sox10^+$-tissue analyses, including disorders of the NC cells and peripheral nerves. The ability to visualize the processes of disease initiation and progression will help to shed light on the pathophysiology of many human diseases.

Conclusions

We developed the novel *Sox10*-Venus BAC transgenic mouse line, in which Venus fluorescence labels NC and oligodendroglial lineage cells. Endogenous Sox10 expression is accurately reported by Venus fluorescence over the course of normal development, without ectopic Venus expression. The highly intense reporter fluorescence allows for *in vivo* imaging of single-cell migration. This strain will be especially useful for analyzing spinal cord injury and studying NCSCs.

Methods

BAC Construction and development of *Sox10*-venus BAC transgenic mice

For generating the *Sox10*-Venus transgenic mouse, we prepared the following BAC construction. Detailed procedures will be described elsewhere (CA, TI, YUI, manuscript in preparation). Briefly, a BAC clone *RP24-85O14* (CHORI, BACPAC Resources) that covers 225.6 kb territory of mouse *Sox10* gene locus was electroporated into the recombinogenic bacterial strain EL250 for systematic modifications [40]. To obtain in-frame replacement of the exon containing the *Sox10* translation initiation codon (ATG) to the Venus-polyadenylation signal (pA) cassette in the BAC clone, 1.2 kb homology arms were amplified by PCR and sequentially subcloned into the pBluescriptII vector (Stratagene). Then the Venus-pA-FRT-*Kanamycin*-resistant gene (*Kan*^{r})-FRT cassette was inserted in between the arms and the fragment containing the Venus-pA-*Kan*^{r} cassette with the homology arms was isolated by agarose gel electrophoresis for homologous recombination which was processed in EL250 as was reported previously [41]. Precise insertion of the Venus-pA cassette and excision of the *Kan*^{r} in the *Sox10*-BAC was verified by PCR as well as pulse field gel electrophoresis and the modified BAC clone was linearlized by PI-*Sce*I, dialyzed and diluted to ~2 ng/μl for pronuclear injections as previously described [41]. For BAC transgenic mouse founders, presence of *RP24* BAC vector sequences immediately upstream or downstream of the PI-*Sce*I site was always examined by PCR tail DNA analyses to minimize the possibility that fortuitous deletions occur on the BAC transgene after the chromosomal integrations [41]. The established BAC transgenic mouse lines were bred with wild-type C57BL/6J mice and the tail DNA was used for the PCR genotyping: The PCR primers for the transgene detections are provided in Table S1; Additional File 5.

Animals

We purchased wild-type C57BL/6J and ICR mice from SLC Japan. The Cre-expressing transgenic lines, *Wnt1*-Cre [14] and *P0*-Cre [15], were mated with an EGFP reporter line (CAG-CAT-EGFP [18]) to obtain *Wnt1*-Cre/CAG-CAT-EGFP and *P0*-Cre/CAG-CAT-EGFP double-transgenic mice. All mice were housed under specific pathogen-free conditions. All experimental procedures were approved by the Institutional Animal Care and Use Committee of Keio University, Murayama Medical Center, and Tokyo Medical and Dental University. All surgical interventions and animal care procedures were in accordance with the Laboratory Animal Welfare Act, the Guide for the Care and Use of Laboratory Animals (National Institute of Health, USA).

Histological analysis

Immunohistochemical analyses were performed as described previously [5,42,43]. Briefly, E9.5 d, n = 3; E10.5 d, n = 10; E11.5 d, n = 9; E12.5 d, n = 5; E13.5 d, n = 6; E14.5 d, n = 3; E15.5 d, n = 7; E16.5 d, n = 3; P0 d, n = 3; and P1 w, n = 3 transgenic embryos (E0 = day of plug) and pups were fixed with 4% PFA, and 16-μm-thick cryosections were prepared with the cryostat CM3000 (Leica). The detailed information about the primary and secondary antibodies was described in Table S1; Additional File 5. Antigen retrieval was applied for specific targets (anti-Olig2, anti-hSox10) by incubating them with Target Retrieval Solution (Dako) in an autoclave at 105°C for 5 minutes. Fluorescence immunostaining with specific primary antibodies was performed overnight at 4° C, followed by one-hour incubation at room temperature with the appropriate secondary antibodies conjugated with Alexa488, Alexa555, or Alexa647 (Invitrogen) along with Hoechst 33258 (10 μg/ml, Sigma) for nuclear staining. The samples were examined with a laser scanning confocal microscope (LSM700 or Pascal: Carl Zeiss) or fluorescent microscope (BZ-9000: Keyence, MVX-CSU: Olympus).

Time-Lapse Imaging

Time-lapse observation (Figure 1G, movies in Additional Files 2 and 3) was performed as described previously [44,45]. Briefly, freshly isolated embryos were collected in cold phosphate buffered saline (PBS) and genotyped based on their Venus fluorescence, using an inverted epifluorecence microscope (Leica MZ10F). The embryos were transferred with 100 - 150 μl of enriched medium to the center of a 35-mm glass-bottom dish (hole size 27 mm; Matsunami) and mixed with 100-150 μl of type I collagen-gel solution (Cellmatrix IA; Nitta Gelatin). The solution had been previously diluted to 0.5-0.6 mg/ml with distilled water, 5× DMEM, and a neutralizing buffer, with a final concentration about 0.3 mg/ml, according to the manufacturer's protocol. The gel was incubated at 37° C for 20 minutes. Once the gel was solidified, up to 600 μl of imaging culture medium was gently added to

the gel. The final concentration of the culture medium was as follows: DMEM/F-12 (1:1), glucose (0.6%), L-glutamine (2 mM), sodium bicarbonate (3 mM), HEPES buffer (50 mM), insulin (25 μg/ml), transferrin (100 μg/ml), progesterone (20 nM), sodium selenate (30 nM), and putrescine (60 μM), with equilibration buffer supplemented with 4% fetal bovine serum. The dish was attached to a pre-heated microscope stage and incubated at 37°C in 5% CO_2. Imaging was carried out with an epifluorescence microscope from Keyence (BZ9000) or a confocal Carl Zeiss microscope (LSM5 PASCAL Exciter). Images were acquired with a 10× objective lens every 10 or 20 minutes, and processed using the Keyence Bz-II application and Zeiss LSM5 software, respectively. NIH ImageJ 1.44e and Quicktime Pro 7.6.8 were used for preparing movie files.

Spinal cord injury model

Adult female *Sox10*-Venus mice (8-weeks old, n = 4 for each time point) were anesthetized with an intraperitoneal injection of ketamine (100 mg/kg) and xylazine (10 mg/kg). The dorsal surface of the dura mater was exposed after laminectomy at the tenth thoracic vertebra, and SCI was induced using an IH (Infinite Horizon) impactor (60 kDyn; Precision Systems & Instrumentation) as described previously [46,47]. The mice were returned to their home cages with free access to water and food. Intact mice and mice at 4 and 14 days post-injury (dpi) were deeply anesthetized and transcardially perfused with chilled PBS followed by 4% paraformaldehyde (PFA). The spinal cords were removed and immersed in 4% PFA at 4°C overnight, and then immersed in 15% and 30% sucrose for 24 hours each, at 4°C. The spinal cords were then embedded in OCT compound and sectioned into 12-μm-thick sagittal sections by cryostat (Leica CM3000).

Additional material

Additional file 1: Embryonic age-dependent fluorescence changes compared among the *Sox10*-Venus, P0-Cre/CAG-CAT-EGFP, and *Wnt1*-Cre/CAG-CAT-EGFP mouse strain. (A-C) Venus fluorescence changes over time were observed from outside of the *Sox10*-Venus embryo. Deep-tissue fluorescence gradually decreased from E11.5 d to E15.5 d (see Figure 1 for additional photos). (C-E) At E14.5 d, reporter gene expression patterns were quite similar between the transgenic *Sox10*-Venus mouse and the double-transgenic mice *P0*-Cre/CAG-CAT-EGFP and *Wnt1*-Cre/CAG-CAT-EGFP. Scale bars (A-E) 1.0 mm.

Additional file 2: Live imaging of single-cell movement: *Sox10*-Venus$^+$ NC-derivatives in the superficial embryonic skin layer (1). Time-lapse imaging with an epifluorescence microscope (Keyence) showed Venus-positive cell movements in E14.5 d *Sox10*-Venus embryo ex-vivo skin explants. One frame was captured every 10 minutes over a 6-hour period (motion: 6 fps).

Additional file 3: Live imaging of single-cell movement: *Sox10*-Venus$^+$ neural crest derivatives in the superficial embryonic skin layer (2). Confocal time-lapse imaging of the front facial area of the whole E10.5 d *Sox10*-Venus embryo captured isolated Venus-positive cells. The distinctive, intense Venus fluorescence made it possible to follow migrating cells within the embryo over several hours, even capturing the dynamic changes in cell shape. One frame was captured every 20 minutes using a confocal Pascal microscope (Carl Zeiss). Scale bar: 50 μm, motion: 4 fps.

Additional file 4: NC progeny were permanently EGFP-labeled in the *Wnt1*-Cre/CAG-CAT-EGFP mouse. (A-B) Immunohistochemical analysis with anti-GFP and marker antibodies for specific cell types showed that the EGFP reporter gene is continuously expressed in NC derivatives in the DRG (A) and sympathetic ganglia (B) of E15.5 d *Wnt1*-Cre/CAG-CAT-EGFP mice. Scale bars (A-B) 50 μm.

Additional file 5: Table S1: Detailed information about sequences and antibodies.

Abbreviations

NC: neural crest; OPC: oligodendrocyte progenitor cell; HMG: high mobility group; PNS: peripheral nervous system; CNS: central nervous system; P0: protein zero; EGFP: enhanced green fluorescent protein; CNP: 2'-3'-cyclic nucleotide 3'-phosphodiesterase; PLP: myelin proteolipid protein; TH: tyrosine hydroxylase; DRG: dorsal root ganglia; SCI: spinal cord injury; DPI: days-post-injury; p75: p75 neurotrophin receptor; NSPC: neural stem/progenitor cell; NCSCs: neural crest stem cells; PBS: phosphate buffered saline.

Acknowledgements

We are grateful to Dr. R.B. Darnell for the gift of the anti-Hu antibody. We are grateful to Drs. C. Hara, N. Kishi, N. Shimojima, M. Mori, A. Iwanami, and H. Kanki for their excellent technical instruction and for critical reading of the manuscript. We also thank all the members in the Okano Laboratory and Akazawa Laboratory for their encouragement and invaluable comments on this manuscript.

This work was supported by a Grant-in-Aid for Young Scientists and a Grant-in-Aid for Scientific Research (C) from The Ministry of Education, Culture, Sports, Science and Technology, Japan (MEXT) to S.S. and F.R-M.; by a Keio University Grant-in-Aid for the Encouragement of Young Medical Scientists to S.S. and F.R-M.; by Keio Gijuku Academic Development Funds to S.S.; by a JST-SORST fellowship to F.R-M.; by grants from Research Foundation ITSUU Laboratory and Takeda Science Foundation to T. I.; and by a Grant-in-Aid from the Global COE Program of the MEXT to Keio University to H.O.

Author details

[1]Department of Physiology, Keio University School of Medicine, Shinjuku-ku, Tokyo 160-8582, Japan. [2]Department of Orthopaedic Surgery, Keio University School of Medicine, Shinjuku-ku, Tokyo 160-8582, Japan. [3]Clinical Research Center, National Hospital Organization, Murayama Medical Center, 2-37-1 Gakuen, Musashimurayama, Tokyo 208-0011, Japan. [4]Department of Biochemistry and Cellular Biology, National Institute of Neuroscience, NCNP, Tokyo 187-8502, Japan. [5]Department of Biochemistry and Biophysics, Graduate School of Health and Sciences, Tokyo Medical and Dental University, Bunkyo, Tokyo, Japan.

Authors' contributions

SS, CA, and HO designed the project. SS, AY, FRM, SS, TI, YUI, NN, and MS performed experiments and analyzed the data. SS, AY, and FRM prepared the figures. SS, AY, FRM, HK, TI, MN, CA, and HO wrote the manuscript. MN, CA, and HO supervised the project. All authors read and approved the final manuscript.

Competing interests

The authors declare that they have no competing interests.

Received: 23 October 2010 Accepted: 31 October 2010
Published: 31 October 2010

References

1. Le Douarin NM, Kalcheim C: *The Neural Crest*. 2 edition. New York, NY: Cambridge University Press; 1999.

2. Le Douarin NM, Creuzet S, Couly G, Dupin E: **Neural crest cell plasticity and its limits.** *Development* 2004, **131**:4637-4650.
3. Le Douarin NM, Dupin E: **Multipotentiality of the neural crest.** *Curr Opin Genet Dev* 2003, **13**:529-536.
4. Morikawa S, Mabuchi Y, Niibe K, Suzuki S, Nagoshi N, Sunabori T, Shimmura S, Nagai Y, Nakagawa T, Okano H, Matsuzaki Y: **Development of mesenchymal stem cells partially originate from the neural crest.** *Biochem Biophys Res Commun* 2009, **379**:1114-1119.
5. Nagoshi N, Shibata S, Kubota Y, Nakamura M, Nagai Y, Satoh E, Morikawa S, Okada Y, Mabuchi Y, Katoh H, *et al*: **Ontogeny and multipotency of neural crest-derived stem cells in mouse bone marrow, dorsal root ganglia, and whisker pad.** *Cell Stem Cell* 2008, **2**:392-403.
6. Bowles J, Schepers G, Koopman P: **Phylogeny of the SOX family of developmental transcription factors based on sequence and structural indicators.** *Dev Biol* 2000, **227**:239-255.
7. Wegner M: **From head to toes: the multiple facets of Sox proteins.** *Nucleic Acids Res* 1999, **27**:1409-1420.
8. Haldin CE, LaBonne C: **SoxE factors as multifunctional neural crest regulatory factors.** *Int J Biochem Cell Biol* 2010, **42**:441-444.
9. Kuhlbrodt K, Schmidt C, Sock E, Pingault V, Bondurand N, Goossens M, Wegner M: **Functional analysis of Sox10 mutations found in human Waardenburg-Hirschsprung patients.** *J Biol Chem* 1998, **273**:23033-23038.
10. Southard-Smith EM, Kos L, Pavan WJ: **Sox10 mutation disrupts neural crest development in Dom Hirschsprung mouse model.** *Nat Genet* 1998, **18**:60-64.
11. Inoue K, Khajavi M, Ohyama T, Hirabayashi S, Wilson J, Reggin JD, Mancias P, Butler IJ, Wilkinson MF, Wegner M, Lupski JR: **Molecular mechanism for distinct neurological phenotypes conveyed by allelic truncating mutations.** *Nat Genet* 2004, **36**:361-369.
12. Inoue K, Tanabe Y, Lupski JR: **Myelin deficiencies in both the central and the peripheral nervous systems associated with a SOX10 mutation.** *Ann Neurol* 1999, **46**:313-318.
13. Pingault V, Bondurand N, Kuhlbrodt K, Goerich DE, Prehu MO, Puliti A, Herbarth B, Hermans-Borgmeyer I, Legius E, Matthijs G, *et al*: **SOX10 mutations in patients with Waardenburg-Hirschsprung disease.** *Nat Genet* 1998, **18**:171-173.
14. Danielian PS, Muccino D, Rowitch DH, Michael SK, McMahon AP: **Modification of gene activity in mouse embryos in utero by a tamoxifen-inducible form of Cre recombinase.** *Curr Biol* 1998, **8**:1323-1326.
15. Yamauchi Y, Abe K, Mantani A, Hitoshi Y, Suzuki M, Osuzu F, Kuratani S, Yamamura K: **A novel transgenic technique that allows specific marking of the neural crest cell lineage in mice.** *Dev Biol* 1999, **212**:191-203.
16. Pietri T, Eder O, Blanche M, Thiery JP, Dufour S: **The human tissue plasminogen activator-Cre mouse: a new tool for targeting specifically neural crest cells and their derivatives in vivo.** *Dev Biol* 2003, **259**:176-187.
17. Soriano P: **Generalized lacZ expression with the ROSA26 Cre reporter strain.** *Nat Genet* 1999, **21**:70-71.
18. Kawamoto S, Niwa H, Tashiro F, Sano S, Kondoh G, Takeda J, Tabayashi K, Miyazaki J: **A novel reporter mouse strain that expresses enhanced green fluorescent protein upon Cre-mediated recombination.** *FEBS Lett* 2000, **470**:263-268.
19. Yoshida S, Shimmura S, Nagoshi N, Fukuda K, Matsuzaki Y, Okano H, Tsubota K: **Isolation of multipotent neural crest-derived stem cells from the adult mouse cornea.** *Stem Cells* 2006, **24**:2714-2722.
20. Tomita Y, Matsumura K, Wakamatsu Y, Matsuzaki Y, Shibuya I, Kawaguchi H, Ieda M, Kanakubo S, Shimazaki T, Ogawa S, *et al*: **Cardiac neural crest cells contribute to the dormant multipotent stem cell in the mammalian heart.** *J Cell Biol* 2005, **170**:1135-1146.
21. Aihara Y, Hayashi Y, Hirata M, Ariki N, Shibata S, Nagoshi N, Nakanishi M, Ohnuma K, Warashina M, Michiue T, *et al*: **Induction of neural crest cells from mouse embryonic stem cells in a serum-free monolayer culture.** *Int J Dev Biol* 2010, **54**:1287-1294.
22. Mallon BS, Shick HE, Kidd GJ, Macklin WB: **Proteolipid promoter activity distinguishes two populations of NG2-positive cells throughout neonatal cortical development.** *J Neurosci* 2002, **22**:876-885.
23. Yuan X, Chittajallu R, Belachew S, Anderson S, McBain CJ, Gallo V: **Expression of the green fluorescent protein in the oligodendrocyte lineage: A transgenic mouse for developmental and physiological studies.** *Journal of Neuroscience Research* 2002, **70**:529-545.
24. Britsch S, Goerich DE, Riethmacher D, Peirano RI, Rossner M, Nave KA, Birchmeier C, Wegner M: **The transcription factor Sox10 is a key regulator of peripheral glial development.** *Genes Dev* 2001, **15**:66-78.
25. Ludwig A, Schlierf B, Schardt A, Nave KA, Wegner M: **Sox10-rtTA mouse line for tetracycline-inducible expression of transgenes in neural crest cells and oligodendrocytes.** *genesis* 2004, **40**:171-175.
26. Stine ZE, Huynh JL, Loftus SK, Gorkin DU, Salmasi AH, Novak T, Purves T, Miller RA, Antonellis A, Gearhart JP, *et al*: **Oligodendroglial and pan-neural crest expression of Cre recombinase directed bySox10enhancer.** *genesis* 2009, **47**:765-770.
27. Nagai T, Ibata K, Park ES, Kubota M, Mikoshiba K, Miyawaki A: **A variant of yellow fluorescent protein with fast and efficient maturation for cell-biological applications.** *Nat Biotechnol* 2002, **20**:87-90.
28. Breuskin I, Bodson M, Thelen N, Thiry M, Borgs L, Nguyen L, Lefebvre PP, Malgrange B: **Sox10 promotes the survival of cochlear progenitors during the establishment of the organ of Corti.** *Developmental Biology* 2009, **335**:327-339.
29. Breuskin I, Bodson M, Thelen N, Thiry M, Borgs L, Nguyen L, Stolt C, Wegner M, Lefebvre PP, Malgrange B: **Glial but not neuronal development in the cochleo-vestibular ganglion requires Sox10.** *J Neurochem* 2010, **114**:1827-1839.
30. Lytle JM, Chittajallu R, Wrathall JR, Gallo V: **NG2 cell response in the CNP-EGFP mouse after contusive spinal cord injury.** *Glia* 2009, **57**:270-285.
31. Brault V, Moore R, Kutsch S, Ishibashi M, Rowitch DH, McMahon AP, Sommer L, Boussadia O, Kemler R: **Inactivation of the beta-catenin gene by Wnt1-Cre-mediated deletion results in dramatic brain malformation and failure of craniofacial development.** *Development* 2001, **128**:1253-1264.
32. Chai Y, Jiang X, Ito Y, Bringas P Jr, Han J, Rowitch DH, Soriano P, McMahon AP, Sucov HM: **Fate of the mammalian cranial neural crest during tooth and mandibular morphogenesis.** *Development* 2000, **127**:1671-1679.
33. Kirby BB, Takada N, Latimer AJ, Shin J, Carney TJ, Kelsh RN, Appel B: **In vivo time-lapse imaging shows dynamic oligodendrocyte progenitor behavior during zebrafish development.** *Nature Neuroscience* 2006, **9**:1506-1511.
34. Takada N, Kucenas S, Appel B: **Sox10 is necessary for oligodendrocyte survival following axon wrapping.** *Glia* 2010, **58**:996-1006.
35. Crane JF, Trainor PA: **Neural crest stem and progenitor cells.** *Annu Rev Cell Dev Biol* 2006, **22**:267-286.
36. Delfino-Machin M, Chipperfield TR, Rodrigues FS, Kelsh RN: **The proliferating field of neural crest stem cells.** *Dev Dyn* 2007, **236**:3242-3254.
37. Aki R, Amoh Y, Li L, Katsuoka K, Hoffman RM: **Nestin-expressing interfollicular blood vessel network contributes to skin transplant survival and wound healing.** *J Cell Biochem* 2010, **110**:80-86.
38. Jinno H, Morozova O, Jones KL, Biernaskie JA, Paris M, Hosokawa R, Rudnicki MA, Chai Y, Rossi F, Marra MA, Miller FD: **Convergent Genesis of an Adult Neural Crest-Like Dermal Stem Cell From Distinct Developmental Origins.** *Stem Cells* 2010.
39. Amoh Y, Li L, Katsuoka K, Hoffman RM: **Multipotent hair follicle stem cells promote repair of spinal cord injury and recovery of walking function.** *Cell Cycle* 2008, **7**:1865-1869.
40. Lee EC, Yu D, Martinez de Velasco J, Tessarollo L, Swing DA, Court DL, Jenkins NA, Copeland NG: **A highly efficient Escherichia coli-based chromosome engineering system adapted for recombinogenic targeting and subcloning of BAC DNA.** *Genomics* 2001, **73**:56-65.
41. Inoue T, Inoue YU, Asami J, Izumi H, Nakamura S, Krumlauf R: **Analysis of mouse Cdh6 gene regulation by transgenesis of modified bacterial artificial chromosomes.** *Dev Biol* 2008, **315**:506-520.
42. Sakakibara S, Nakamura Y, Satoh H, Okano H: **Rna-binding protein Musashi2: developmentally regulated expression in neural precursor cells and subpopulations of neurons in mammalian CNS.** *J Neurosci* 2001, **21**:8091-8107.
43. Sakakibara S, Nakamura Y, Yoshida T, Shibata S, Koike M, Takano H, Ueda S, Uchiyama Y, Noda T, Okano H: **RNA-binding protein Musashi family: roles for CNS stem cells and a subpopulation of ependymal cells revealed by targeted disruption and antisense ablation.** *Proc Natl Acad Sci USA* 2002, **99**:15194-15199.

44. Miyata T, Nakajima K, Mikoshiba K, Ogawa M: **Regulation of Purkinje cell alignment by reelin as revealed with CR-50 antibody.** *J Neurosci* 1997, **17**:3599-3609.
45. Miyata T, Ogawa M: **Twisting of neocortical progenitor cells underlies a spring-like mechanism for daughter-cell migration.** *Curr Biol* 2007, **17**:146-151.
46. Kumagai G, Okada Y, Yamane J, Nagoshi N, Kitamura K, Mukaino M, Tsuji O, Fujiyoshi K, Katoh H, Okada S, *et al*: **Roles of ES cell-derived gliogenic neural stem/progenitor cells in functional recovery after spinal cord injury.** *PLoS One* 2009, **4**:e7706.
47. Scheff SW, Rabchevsky AG, Fugaccia I, Main JA, Lumpp JE Jr: **Experimental modeling of spinal cord injury: characterization of a force-defined injury device.** *J Neurotrauma* 2003, **20**:179-193.

doi:10.1186/1756-6606-3-31
Cite this article as: Shibata *et al.*: *Sox10*-Venus mice: a new tool for real-time labeling of neural crest lineage cells and oligodendrocytes. *Molecular Brain* 2010 **3**:31.

Experimental Neurology 224 (2010) 403–414

Contents lists available at ScienceDirect

Experimental Neurology

journal homepage: www.elsevier.com/locate/yexnr

Anti-IL-6-receptor antibody promotes repair of spinal cord injury by inducing microglia-dominant inflammation

Masahiko Mukaino [a,b], Masaya Nakamura [c,*], Osamu Yamada [b], Seiji Okada [d], Satoru Morikawa [e], Francois Renault-Mihara [b], Akio Iwanami [c,f], Takeshi Ikegami [c,f], Yoshiyuki Ohsugi [g], Osahiko Tsuji [c], Hiroyuki Katoh [f], Yumi Matsuzaki [b], Yoshiaki Toyama [c], Meigen Liu [a], Hideyuki Okano [b,*]

[a] Department of Rehabilitation Medicine, Keio University School of Medicine, Shinjuku, Tokyo 160-8582, Japan
[b] Department of Physiology, Keio University School of Medicine, Shinjuku, Tokyo 160-8582, Japan
[c] Department of Orthopedic Surgery, Keio University School of Medicine, Shinjuku, Tokyo 160-8582, Japan
[d] Department of Research Superstar Program Stem Cell Unit, Graduate School of Medical Science, Kyushu University, Fukuoka 812-8582, Japan
[e] Department of Dentistry and Oral Surgery, Keio University School of Medicine, Shinjuku, Tokyo 160-8582, Japan
[f] National Hospital Organization, Murayama Medical Center, Musashimurayama, Tokyo 208-0011, Japan
[g] Chugai Pharmaceutical Co. Ltd., Chuo, Tokyo 103-8324, Japan

ARTICLE INFO

Article history:
Received 16 October 2009
Revised 29 April 2010
Accepted 30 April 2010
Available online 16 May 2010

Keywords:
Spinal cord injury
Interleukin-6
Antibody
Inflammation
Microglia
Hematogenous macrophages

ABSTRACT

We previously reported the beneficial effect of administering an anti-mouse IL-6 receptor antibody (MR16-1) immediately after spinal cord injury (SCI). The purpose of our present study was to clarify the mechanism underlying how MR16-1 improves motor function after SCI. Quantitative analyses of inflammatory cells using flow cytometry, and immunohistochemistry with bone marrow-chimeric mice generated by transplanting genetically marked purified hematopoietic stem cells, revealed that MR16-1 dramatically switched the central player in the post-traumatic inflammation, from hematogenous macrophages to resident microglia. This change was accompanied by alterations in the expression of relevant cytokines within the injured spinal cord; the expression of recruiting chemokines including CCL2, CCL5, and CXCL10 was decreased, while that of Granulocyte/Macrophage-Colony Stimulating Factor (GM-CSF), a known mitogen for microglia, was increased. We also showed that the resident microglia expressed higher levels of phagocytic markers than the hematogenous macrophages. Consistent with these findings, we observed significantly decreased tissue damage and reduced levels of myelin debris and Nogo-A, the axonal growth inhibitor, by MR16-1 treatment. Moreover, we observed increased axonal regeneration and/or sprouting in the MR16-1-treated mice. Our findings indicate that the functional improvement elicited by MR16-1 involves microglial functions, and provide new insights into the role of IL-6 signaling in the pathology of SCI.

Introduction

In the pathology of spinal cord injury (SCI), the primary mechanical injury is followed by post-traumatic inflammation, in which inflammatory cells such as neutrophils, hematogenous macrophages (blood-borne macrophages), and resident microglia accumulate at the lesion site. These inflammatory cells release reactive oxygen, nitrogen radicals, and proteases, which exacerbate tissue damage (Hausmann, 2003). Because the inflammation is regulated by pro-inflammatory cytokines, such as TNFα, IL-1β, and IL-6, these cytokines have been targets for potential pharmaceutical interventions for SCI (Nesic et al., 2001; Okada et al., 2004; Sharma et al., 2003; Tuna et al., 2001). Among these cytokines, IL-6 is known to promote the activation and infiltration of macrophages/microglia (Hurst et al., 2001; Van Wagoner and Benveniste, 1999), which are the major inflammatory cells in the injured spinal cord, and the overexpression of IL-6 extends the inflammation to worsen the tissue injury (Klusman and Schwab, 1997; Lacroix et al., 2002). Hypothesizing that a blockade of IL-6 signaling might reduce the extension of injury by post-SCI inflammation, we previously administered the anti-mouse IL6-receptor antibody (MR16-1) after SCI and demonstrated reduced inflammation, decreased astrogliosis, and enhanced tissue sparing, leading to improved functional recovery (Okada et al., 2004). As a humanized antibody for the human IL-6 receptor (MRA; tocilizumab) is already in clinical use for the treatment of Castleman's disease and rheumatoid arthritis (Choy et al., 2002; Nishimoto et al., 2000; Sato et al., 1993), this drug might represent a new option for the treatment of SCI.

* Corresponding authors. H. Okano is to be contacted at the Department of Physiology, Keio University School of Medicine, 35 Shinanomachi, Shinjuku, Tokyo 160-8582, Japan. M. Nakamura, Department of Orthopedic Surgery, Keio University School of Medicine, Shinjuku, Tokyo 160-8582, Japan. Fax: +81 3 3357 5445.
E-mail addresses: masa@sc.itc.keio.ac.jp (M. Nakamura), hidokano@sc.itc.keio.ac.jp (H. Okano).

0014-4886/$ – see front matter © 2010 Elsevier Inc. All rights reserved.
doi:10.1016/j.expneurol.2010.04.020

However, recent studies using gene-knockout animals revealed that the continuous inhibition of IL-6 signaling is detrimental to functional recovery, by inhibiting axonal regeneration or causing failed gliosis, implying that IL-6 may also have a beneficial function in spinal cord repair (Cafferty et al., 2004; Okada et al., 2006). Furthermore, numerous studies suggest that inflammation is beneficial or even essential for spinal cord repair, because it clears tissue debris and involves the secretion of various neurotrophic factors (Donnelly and Popovich, 2008; Hashimoto et al., 2005; McTigue et al., 2000). This discrepancy prompted us to investigate how the administration of an anti-IL-6 receptor antibody immediately after SCI promotes the repair process.

One of the important determinants of the extent of secondary damage by inflammation is the nature of the recruited inflammatory cells. For example, the transplantation of macrophages that have been co-incubated with peripheral nerves or skin improves spinal cord repair (Bomstein et al., 2003; Schwartz et al., 1999). On the other hand, zymosan-activated macrophages have neurotoxic properties, although they can also have proregenerative effects (Gensel et al., 2009; Popovich et al., 2002; Steinmetz et al., 2005). Previous reports have shown that these differences in the characteristics of inflammatory cells depend not only on their state of activation, but also on their origin. A subpopulation of hematogenous macrophages is more cytotoxic than microglia, and their excessive infiltration into a lesion is detrimental to spinal cord repair (Gris et al., 2004; Popovich et al., 1999). Since IL-6 is known to promote macrophage infiltration after central nervous system (CNS) trauma (Klusman and Schwab, 1997; Lacroix et al., 2002), here we focused on the effect of the temporary inhibition of IL-6 signaling by MR16-1 on macrophages and microglia after SCI. The administration of MR16-1 reduced the infiltration of macrophages into the injured spinal cord, but increased the number of microglia residing there, thus switching the major inflammatory cell type at the lesion from hematogenous macrophages to resident microglia. A comparison of the expression of phagocytic markers by hematogenous macrophages and microglia revealed that the microglia had greater phagocytic ability against myelin debris after SCI. Consequently, this switch in major inflammatory cell type resulted in improved tissue sparing and debris clearance, which promoted neural repair after SCI.

Materials and methods

Animals

74 adult female C57BL/6J mice (8–10 weeks old) were used. C57BL/6 background CAG-EGFP transgenic mice that ubiquitously express EGFP under the control of the CAG promoter (Kawamoto et al., 2000) were kindly provided by Professor Jun-ichi Miyazaki (Osaka University, Osaka, Japan) and were bred in our animal facility. The ethics committee of our institution approved all the surgical and animal care procedures, in accordance with the Laboratory Animal Welfare Act, the Guide for the Care and Use of Laboratory Animals (National Institutes of Health), and the Guidelines and Policies for Animal Surgery provided by the Animal Study Committees of the Central Institute for Experimental Animals and of Keio University.

Rat anti-mouse IL-6 receptor monoclonal antibody (MR16-1)

The rat anti-mouse IL-6 receptor monoclonal antibody MR16-1 was prepared as described previously (Tamura et al., 1993). MR16-1 binds to the mouse IL-6 receptor and suppresses IL-6-induced cellular responses in a dose-dependent manner (Okazaki et al., 2002). Other basic characterizations of this antibody were reported previously (Okazaki et al., 2002; Tamura et al., 1993).

Purification and transplantation of genetically marked hematopoietic stem cells (HSCs)

In the present study, we produced bone marrow-chimeric mice using highly purified, genetically marked hematopoietic stem cells by the method reported by Koide et al. (2007). This method enabled us to limit our observation specifically to the hematopoietic cell lineage. The femurs and tibias were dissected from donor CAG-EGFP transgenic mice and crushed with a pestle. The marrow cells were collected in HBSS+ (Hanks-balanced salt solution supplemented with 2% FCS, 10 mM HEPES, and 1% penicillin/streptomycin), filtered through a cell strainer (Falcon 2350) to remove debris, and suspended in 50 ml of ice-cold HBSS+. The cells were collected by centrifugation at 280 *g* for 6 min at 4 °C, resuspended in HBSS+ at 1×10^6 cells/ml, and incubated with 5 μg/ml Hoechst 33342 (Sigma Chemical Co.) for 60 min at 37 °C. A parallel aliquot was stained with Hoechst dye in the presence of 50 μM reserpine (Sigma Chemical Co.). The cells were spun down, resuspended in 5 ml of ice-cold HBSS+, and layered on top of 5 ml of Ficoll-Paque™ Plus (Amersham Pharmacia Biotech AB, Uppsala, Sweden). After centrifugation at 630 *g* at 4 °C for 20 min, the mononuclear cells were collected from the intermediate layer and immediately washed with 10 ml of ice-cold HBSS+. The Hoechst-stained cells were resuspended in ice-cold HBSS+ at $1–5\times10^7$ cells/ml and stained for 30 min on ice with one of the following monoclonal antibodies: biotinylated CD34 (RAM34), PE-conjugated Sca-1 (Ly6A/E), or APC-conjugated c-Kit (2B8). Biotinylated antibodies were visualized with Cy7-APC-conjugated streptavidin. All of these reagents were purchased from eBioscience (San Diego, CA). An aliquot of cells was also stained with a mouse isotype control conjugated with FITC, PE, or APC. After antibody staining, the cells were washed in an excess volume of HBSS+ and resuspended at 1×10^7 cells/ml in HBSS+ containing 2 μg/ml propidium iodide (PI; Sigma Chemical Co.). Genetically marked, highly purified HSCs ($CD34^-$ $Sca\text{-}1^+$ $c\text{-}kit^+$ SP cells (Matsuzaki et al., 2004)) derived from donor CAG-EGFP transgenic animals were sorted by flow cytometry. A 100-μl aliquot of unfractionated marrow cell suspension (2×10^5 cells) from donors not carrying the CAG-EGFP transgene was added to provide competitor cells, which is the minimum dose to keep the animals alive during the period required for bone marrow reconstitution. A suspension of 100 $CD34^-$ $Csa\text{-}1^+$ $c\text{-}kit^+$ SP cells and 2×10^5 unfractionated marrow cells was then intravenously injected into the retro-orbital plexus of an etherized recipient mouse that had been lethally irradiated at 10.5 Gy. The successful induction of chimerism was confirmed by a Dual-laser FACS Calibur (Becton and Dickinson, CA) analysis of the peripheral blood.

Spinal cord injury model

Mice were anesthetized with an intraperitoneal injection of ketamine (100 mg/kg) and xylazine (10 mg/kg). The dorsal surface of the dura mater at the T10 level was exposed by laminectomy, and a moderate (impact force = 60 kdyn) contusion injury was induced using an IH impactor, as reported previously (Cafferty et al., 2004; Glass et al., 2001). The muscles and skin were closed in layers, and the animals were placed in a temperature-controlled chamber until thermoregulation was reestablished. Manual voiding of the bladder was performed twice per day until reflex bladder emptying was reestablished.

Injection of MR16-1 and BrdU

Immediately after SCI, mice were given a single intraperitoneal injection of MR 16-1 (100 μg/g body weight; MR16-1-treated group) or the same volume and concentration of purified rat IgG (ICN/Cappel Ohio; control group). To label the cells that divided after the injury, a sterile solution of bromodeoxyuridine (BrdU; 50 μg/g body weight; Sigma) was injected intraperitoneally immediately after the injury, and then every 24 h for 4 days after SCI (a total of 5 times).

Immunohistochemistry

At 4, 7, 14, and 42 days after SCI, animals in the MR16-1-treated and control groups were deeply anesthetized by inhalation of diethyl ether and transcardially perfused with 4% paraformaldehyde in 0.1 M phosphate-buffered saline (PBS). The spinal cord tissue was removed and post-fixed in 4% paraformaldehyde in PBS for a few hours at room temperature. The tissue samples were immersed in 10% sucrose in PBS at 4 °C for 24 h, then placed in 30% sucrose in PBS for 48 h, and embedded in OTC compound. The embedded tissue was immediately frozen in liquid nitrogen and stored at −80 °C until use. Frozen spinal cord tissues were sectioned on a cryostat at 20 μm, either in the axial or sagittal plane. Luxol fast blue and Oil red O staining were performed to evaluate the spared myelin and myelin debris.

For immunohistochemistry with fluorescent antibodies, spinal cord sections were permeabilized with 0.03% Triton X-100 and 10% normal goat serum in 0.01 M PBS, pH 7.4, for 30 min. The following primary antibodies were applied overnight at 4 °C: rat anti-CD11b, 1:200 (Serotec, Oxford, United Kingdom); rabbit anti-Iba-1, 1:200 (Wako Pure Chemical Industries, Osaka, Japan); rat anti-LAMP2, 1:200 (Abcam, Cambridge, UK); rat anti-Mac2, 1:200 (Cedarlane, Hornby, Ontario); rabbit anti-GFP, 1:500 (MBL, Nagoya, Japan); goat anti-GFP, 1:500 (Rockland Immunochemicals, Gilbertsville, PA); or chick anti-GFP, 1:500 (Aves Lab, Tigard, OR). The sections were then incubated for 1 h at room temperature with secondary antibodies conjugated with Texas red or fluorescein isothiocyanate (FITC; all from Jackson Immunoresearch, West Grove, PA). The sections were then washed, wet-mounted, and examined by epi-fluorescence. Multiple staining with Oil red O was performed by the method reported by Koopman et al. (2001).

For diaminobenzidine (DAB; Sigma) staining, mouse anti-Neurofilament 200kD antibody, 1:200 (Chemicon, Temecula, CA) or goat anti-5HT, 1:200 (Immunostar, Hudson, WI) was used as the primary antibody, followed by horseradish peroxidase (HRP)-labeled goat anti-mouse IgG or donkey anti-goat IgG as the secondary antibody. The staining was visualized with DAB, and the sections were washed, dehydrated, cleared in xylene, and mounted.

Quantitative analyses

For quantitative analyses, three representative midsagittal or axial sections through the injured portion of the spinal cord of each mouse were selected randomly and captured at 50× magnification. The areas of tissue immunopositive for CD11b, Iba-1, LAMP2, Mac2, Neurofilament 200kD, and Nogo-A, and those stained with Oil red O (ORO) and Luxol Fast Blue (LFB) were quantified using the ImageJ software and MCID system (Imaging Research, Inc., St. Catharines, Ontario, Canada). To count the number of macrophages/microglia, three midsagittal sections through the injured portion of the spinal cord of each mouse were selected randomly, and the number of CD11b- or Iba-1- and/or EGFP-immunopositive cells contained within a cephalocaudal stretch of 500 μm at the indicated levels was counted. To confirm the CD11b-Iba-1 double-staining as a marker of macrophages/microglia the ratio of CD11b-Iba-1 double-stained cells to total CD11b-positive cells was also quantified. To count the LAMP2- andMac2-positive cells, three midsagittal sections through the injured portion of the spinal cord of each mouse were selected randomly, and a threshold was determined from the basal fluorescence of a portion of intact tissue. From the epicenter area (0–1-mm caudal and rostral to the epicenter), 15 non-overlapping high-power fields were chosen at random (630× magnification; total area 0.39 mm^2). An immunopositive cell was defined as a cell with staining over 10% of its soma, as determined by the MCID system, and the number of stained and unstained cells was counted manually. For the quantification of $5HT^+$ fibers, five regions (the dorsal horn and ventral horn of both sides, and the site around the central canal) from each axial section of the cord, 2-mm caudal to the epicenter, were captured at ×200 magnification, and the area of the $5HT^+$ tissue in each field was quantified using the MCID system. The light intensity and threshold values were maintained at constant levels for all analyses.

Flow cytometry

Mice were transcardially perfused with 0.1 M phosphate-buffered saline, and the spinal cords were harvested. The injured portion of each spinal cord (6 mm) was surgically dissected, digested with collagenase, mechanically homogenized, and passed through a wire mesh screen (Sigma-Aldrich Canada Ltd., Ontario, Canada) to obtain a single-cell suspension. The cells were washed in PBS containing 3% FBS, and incubated for 5 min on ice with Fc Block and 30 min on ice with fluorescent antibodies. Flow cytometric analysis was performed using a FACS Calibur (Becton Dickinson) and MoFlo (Dakocytomation), and the data were analyzed using Cell Quest software. The cells were stained with antibodies against CD11b-PE, CD45-FITC, and CD45-APC (eBioscience, San Diego, CA), and were classified according to their expression level of CD45 (common leukocyte antigen) and CD11b (complement 3 receptor), with $CD11b^+$ $CD45^{high}$ indicating hematogenous macrophages and $CD11b^+$ $CD45^{low}$ indicating resident microglia, as reported previously (Sedgwick et al., 1991). At least 1.0×10^6 cells were analyzed for each spinal cord sample.

Western blot analysis

Twenty-four hours after the injury, the spinal cord tissue at the lesion epicenter (6 mm in length) was dissected from the mice (four animals per group and four sham-operated animals), homogenized in MAPK lysis buffer containing protease inhibitors, sonicated, and spun at 15,000 rpm. The proteins in the supernatants were separated by 10% SDS-PAGE and transferred to a polyvinylidene difluoride membrane by electrophoresis. The membranes were blocked for 1 h at room temperature in TBST buffer containing 4% non-fat milk, NaCl (150 mM), and 0.05% Tween 20. The blots were then incubated with primary polyclonal rabbit anti-CCL2 antibody (1:2000; Abcam, Cambridge, MA), goat anti-CCL5 antibody, 1:500 (eBioscience, San Diego, CA); rabbit anti-CXCL-10 antibody, 1:500 (Cedarlane, Hornby, Ontario); rabbit anti-GM-CSF antibody, 1:2000 (Abcam, Cambridge, MA); or mouse anti-α-tubulin antibody, 1:500 followed by a secondary HRP-conjugated anti-rabbit, goat, or mouse IgG antibody. The blots were visualized with the ECL Blotting Analysis System (Amersham, Arlington Heights, IL).

Real time RT-PCR

A 4-mm-long spinal cord segment at T10 was collected at the indicated times, the total RNA was isolated using an RNeasy Kit (Qiagen Science, Maryland, USA), and cDNA was obtained by reverse transcription. The cDNA synthesis was performed at 42 °C for 50 min in a final volume of 20 μl, following the manufacturer's instructions for Superscript II RNase H Reverse Transcriptase (Invitrogen). The template cDNA was normalized to the β-actin mRNA. Real time RT-PCR was performed using an Mx3000P thermal cycler (Stratagene) with SYBR green (TaKaRa RR041A). For every set of RT-PCR analyses, at least three independent experiments were performed. The amplification was performed using the following primers: CCL2, sense 5′-GCATCCACGTGTTGGCTCA-3′, antisense 5′-CTCCAGCCTACTCATTGGGATCA-3′; CCL5, sense 5′-AGATCTCTGCAGCTGCCCTCA-3′, antisense 5′-GGAGCACTTGCTGCTGGTGTAG-3′; CXCL10, sense 5′-TGAATCCGGA ATCTAAGACCATCAA-3′, antisense 5′-AGGACTAGCCATCCACTGG GTAAAG-3′ (purchased from Takara, Kyoto, Japan) and GM-CSF, sense 5′-AAGGTCCTGAGGAGGA TGTG-3′, antisense 5′-GAGGTTCAGGGCTTCTTTGA-3′ (purchased from Hokkaido System Science, Sapporo, Japan).

Statistical analysis

Values are reported as the mean ± SEM. Statistical significance was analyzed using the unpaired Student's *t*-test, and significance was accepted at $P<0.05$.

Results

Anti-IL-6 receptor antibody treatment reduced inflammatory cell accumulation

To examine the effect of MR16-1 on the infiltration of inflammatory cells after SCI, immunostaining for CD11b and Iba-1 was performed. Although CD11b is known to be expressed by granulocytes and some T cells, 93.6 ± 3.3% of the infiltrated cells were CD11b and Iba-1 double-positive at 4, 7, and 14 days post-injury (dpi), indicating that the immunocompetent cells present at the injured site at those times after SCI were mostly hematogenous macrophages and resident microglia (Figs. 1A–E). While the CD11b-positive area increased in both the MR16-1 and control groups, with a peak at 7 dpi, the MR16-1-treated animals showed a significantly smaller CD11b$^+$ area compared to the control animals: a non-significant difference at 4 and 7 dpi that developed to a significant difference at 14 dpi (Fig. 1F). These findings suggest that MR16-1 administration reduced the accumulation of CD11b$^+$ cells at the late stage of inflammation, even though MR16-1 was only administered once, at the acute stage.

To determine whether the administration of MR16-1 alters the subtype of CD11b$^+$ cells at the acute stage, the profiles of the recruited CD11b$^+$ cells were analyzed using flow cytometry. Homogenates of the injured spinal cord were analyzed to determine the ratio of hematogenous macrophages to total CD11b$^+$ cells. We first confirmed that within the CD11b$^+$ population, hematogenous macrophages could be distinguished from the resident microglia by their expression level of CD45, as reported previously (Sedgwick et al., 1991). At 4 dpi, 37.6 ± 3.9% of the CD11b$^+$ cells were CD45^{high} hematogenous macrophages in the control group, whereas only 22.3 ± 2.9% of these cells were CD45^{high} in the MR16-1-treated group. Although the proportion of hematogenous macrophages had increased in both groups at 7 dpi, the difference in their proportions between the MR16-1-treated and control mice was significant (57.8 ± 1.9% in the control group, 41.0 ± 2.2% in the MR16-1-treated group) (Figs. 1G–I). MR16-1 treatment thus reduced the relative abundance of hematogenous macrophages in the injured spinal cord.

MR16-1 treatment caused the central player in the inflammation after SCI to shift from hematogenous macrophages to resident microglia

To determine whether MR16-1 specifically affects the recruitment of hematogenous macrophages into the injured spinal cord, contusive SCI was induced in chimeric mice, which were generated by irradiating

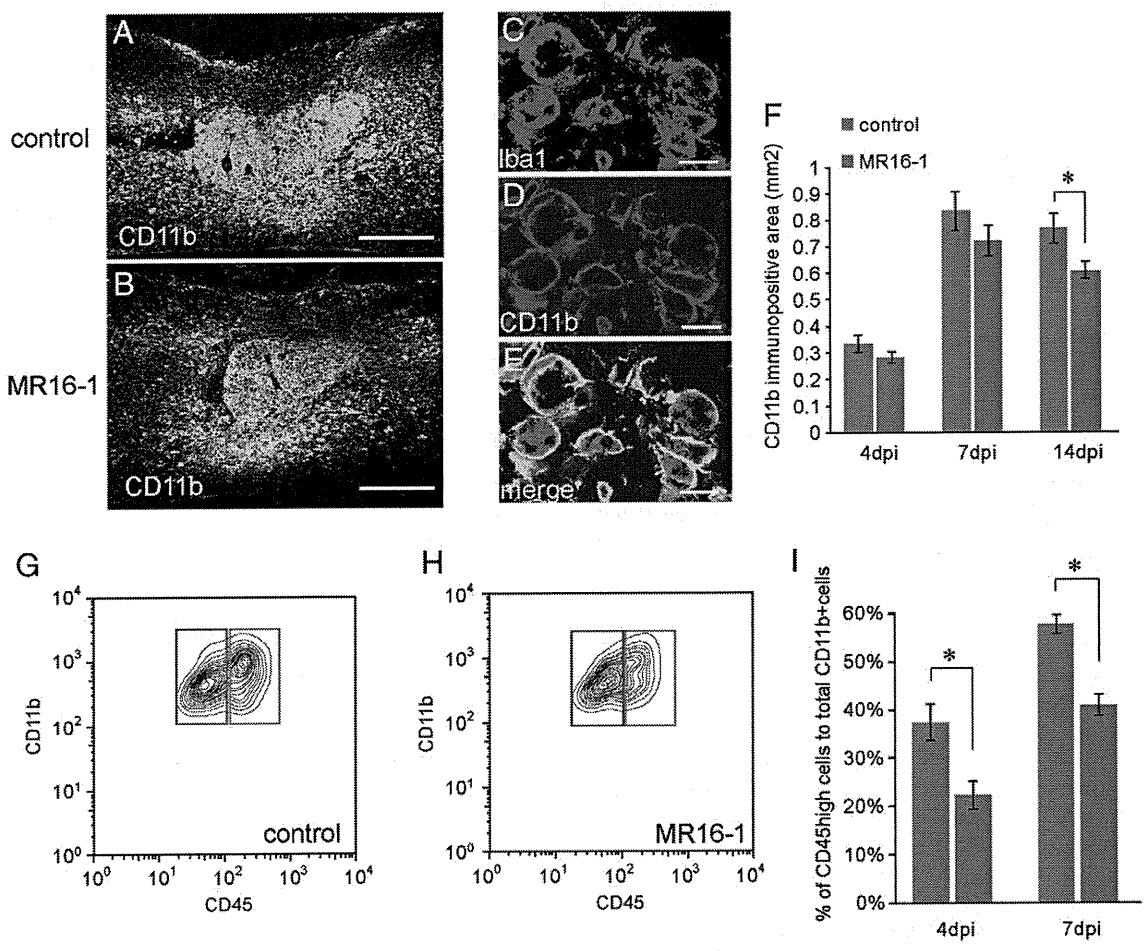

Fig. 1. MR16-1 treatment accelerates the resolution of inflammation. A, B, F: There was a significant difference in the CD11b$^+$ area between the control group (A) and the MR16-1-treated group (B) at 14 dpi, but not at 4 or 7 dpi (F). C–E: 96.9 ± 1.3% of the CD11b$^+$ cells (D) were double-labeled with Iba1 (C, E), indicating that the accumulated CD11b$^+$ cells were inflammatory macrophages/microglia. G–I: MR16-1-treatment decreased the proportion of hematogenous macrophages in the injured spinal cord at 4 and 7 dpi. Hematogenous macrophages (CD11b$^+$CD45^{high}, blue box) and microglia (CD11b$^+$CD45^{low}, red box) were identified according to their levels of CD11b and CD45 expression. I: The proportion of hematogenous macrophages within the CD11b$^+$ population was significantly lower in the MR16-1-treated animals than in the control group at 4 and 7 dpi. Values are means ± SEM. *$P<0.05$. Scale bars = 500 μm in A, B; 20 μm in C–E.

recipient mice and then transplanting purified EGFP-expressing HSCs into them (Matsuzaki et al., 2004). Flow cytometric analysis revealed that 3 months after the HSC transplantation, 88.34±1.45% of the $CD11b^+$ leukocytes in the blood of the chimeric mice were EGFP-positive. In contrast, only 1.57% of the $CD11b^+$ cells in the uninjured spinal cord expressed EGFP, suggesting that the recruitment of microglia from the hematopoietic pool was a rare event. Since the irradiation dose required for this method is rather high (10.5 Gy), which could affect microglial turnover (Mildenberger et al., 1990), we quantified the accumulation of CD11b+ cells at the lesion of chimeric mice, and compared it to that of wild-type mice. There was no significant difference in the number of CD11b+ cells between the chimeric mice and wild-type mice at 4, 7, or 14 dpi ($P=0.60$, 0.76, 0.67, respectively). This result is consistent with the previous report by Turrin et al. (2007), which showed that the chimerization with 10 Gy irradiation dose does not significantly affect the acute inflammatory response. Thus, these chimeric mice enabled us to distinguish in situ hematogenous macrophages from endogenous microglia by their EGFP immunoreactivity (Figs. 2A–C), and examine the precise spatio-temporal localization of these cell populations after SCI.

Consistent with our findings using wild-type mice, the total number of recruited $CD11b^+$ macrophages/microglia was comparable between the MR16-1-treated and control groups at 4 dpi (not shown), but the proportion and distribution of the hematogenous macrophages and microglia were completely different (Figs. 2D, E, G, and I). In the MR16-1-treated group, there were significantly fewer $CD11b^+EGFP^+$ hematogenous macrophages at the lesion site (Fig. 2G), and there were significantly more $CD11b^+EGFP^-$ resident microglia, especially in areas 1.0- to 2.0-mm away from the lesion site (Fig. 2I). Thus, at 4 dpi, the MR16-1 treatment led to a reduced accumulation of hematogenous macrophages at the lesion epicenter, and an increased number of microglia at sites rostral and caudal to the lesion epicenter.

Similarly, at 7 dpi, although the distribution of $CD11b^+$ cells was comparable in the control and MR16-1-treated groups (Fig. 2F), the composition of the $CD11b^+$ population was dramatically different. In the MR16-1-treated group, the $CD11b^+EGFP^+$ hematogenous macrophage accumulation at the lesion epicenter was significantly reduced (Fig. 2H), and the $CD11b^+EGFP^-$ resident microglia had significantly increased (Fig. 2J). These results indicate that the central player in the inflammation after SCI shifted from being hematogenous macrophages to being resident microglia, following MR16-1-treatment.

MR16-1 treatment reduced the expression of macrophage-recruiting chemokines and increased the GM-CSF level at the lesion site

Although there is no evidence that IL-6 directly stimulates the infiltration or proliferation of inflammatory cells, it does affect the expression of various cytokines; furthermore, the blockade of IL-6 signaling during inflammation causes a drastic change in the cytokine profile, including the chemokines and colony-stimulating factors (CSFs) (Matsumura et al., 1999; Romano et al., 1997). Because the infiltration of hematogenous macrophages is mediated by chemokines (Babcock et al., 2003; Romano et al., 1997) and the increased proliferation of microglia is mainly controlled by CSFs (Giulian and Ingeman, 1988; Lee et al., 1994), we examined the expression levels of CCL2 (MCP-1), CCL5 (RANTES), CXCL10 (IP-10), and GM-CSF, which are representative cytokines known to direct cell infiltration and proliferation, by quantitative real time PCR, 12 h after injury. The mRNA levels of CCL2, CCL5, and CXCL10 were significantly attenuated by MR16-1-administration compared to the control group (to 15.0%, 49.7% and 30.8% of the control levels, respectively), whereas the GM-CSF mRNA level was significantly increased (to 214% of the control level) (Figs. 3A–D). We also quantified the cytokine proteins by western blotting. The protein level of CCL2 was significantly decreased (to 80.7% of the control level), whereas the GM-CSF level was significantly increased (to 193% of the control level). Although the difference did not reach to statistical significance, we also observed a tendency for the protein levels of CCL5 and CXCL10 to decrease (Figs. 3E–H).

Microglia had higher phagocytic capacities than hematogenous macrophages

To determine whether the shift in the major inflammatory cells by MR16-1 treatment affected the inflammatory process, we further characterized the hematogenous macrophages and the microglia. The phagocytosis of tissue debris by inflammatory cells is a pivotal process for spinal cord repair after injury, as the debris includes various cytotoxic agents and axonal growth inhibitory factors. Quantitative analysis revealed that the expression of LAMP2, a marker for endosomes/lysosomes, was significantly increased at the lesion epicenter in the MR16-1-treated group compared to the control group, at 4, 7, and 14 dpi (Figs. 4A–C). Previous reports showed that the resident microglia have higher phagocytic activity than the infiltrating hematogenous macrophages (Rinner et al., 1995; Schilling et al., 2005). Consistent with these reports, we found that significantly more $Iba1^+EGFP^-$ resident microglia expressed LAMP2 than did the $Iba1^+EGFP^+$ hematogenous macrophages at 4 and 7 dpi (Figs. 4D–G).

In addition, we performed immunostaining with Mac2, which is reported to participate in the phagocytosis of myelin (Rotshenker et al., 2008). Although Mac2 was expressed on the cell membrane of most of the accumulated cells, only a portion of the macrophages/microglia expressed Mac2 in their cytoplasm. Consistent with the LAMP2 results, more of the $Iba1^+EGFP^-$ resident microglia than $Iba1^+EGFP^+$ hematogenous macrophages showed cytoplasmic expression of Mac2 (Figs. 5A–D, and I). Similarly, the average size and intracellular $Mac2^+$ area of the resident microglia were significantly greater at 7 dpi than those of hematogenous macrophages (Figs. 5J and K). We also performed triple staining for Iba-1, EGFP, and Oil red O using the method reported by Koopman et al. (2001) to observe phagocytosed lipid, which is derived from myelin. The Oil red O^+ area in each cell body was significantly greater in the $Iba1^+EGFP^-$ resident microglia than in the $Iba1^+EGFP^+$ hematogenous macrophages, and was increased at 7 dpi by the MR16-1 treatment (Figs. 5E–H, L).

MR16-1 treatment promotes repair of the spinal cord

To examine the effect of the altered inflammatory response on spinal cord repair, we evaluated the clearance of myelin debris by Oil red O staining and Nogo-A immunostaining, as well as the sparing of myelin sheath, which is evaluated by Luxol Fast Blue staining. At 14 and 42 dpi, the Oil red O^+ area was significantly decreased in the MR16-1-treated group compared to the control group (Figs. 6A–C). The deposition of Nogo-A, the major myelin-derived axonal growth inhibitor, was also decreased by MR16-1 treatment (Figs. 6D–F). Furthermore, we evaluated the spared myelin sheath using Luxol fast blue staining. At the lesion epicenter, the area of the spared myelin sheath in the MR16-1-treated group was significantly greater than in the control group at 14 and 42 dpi (Figs. 6G–I).

To determine the effect of MR16-1 on repair of neural tissue, we quantified the RT-97^+ (Neurofilament 200kD) fibers at the lesion epicenter and the 5-HT^+ (serotonergic) fibers that were caudal to the lesion site. There was no significant difference in the area of RT-97^+ fibers between the two groups at 14 dpi, but a significantly larger RT-97^+ area was observed in the MR16-1-treated group at 42 dpi (Figs. 6J–K). Similarly, there was no significant difference in the 5-HT^+ area between the two groups at 14 dpi. Although there was a slight increase in 5-HT^+ fibers at 42 dpi, even in the control group, which is characteristic of contusive SCI, a significantly larger area of 5-HT^+

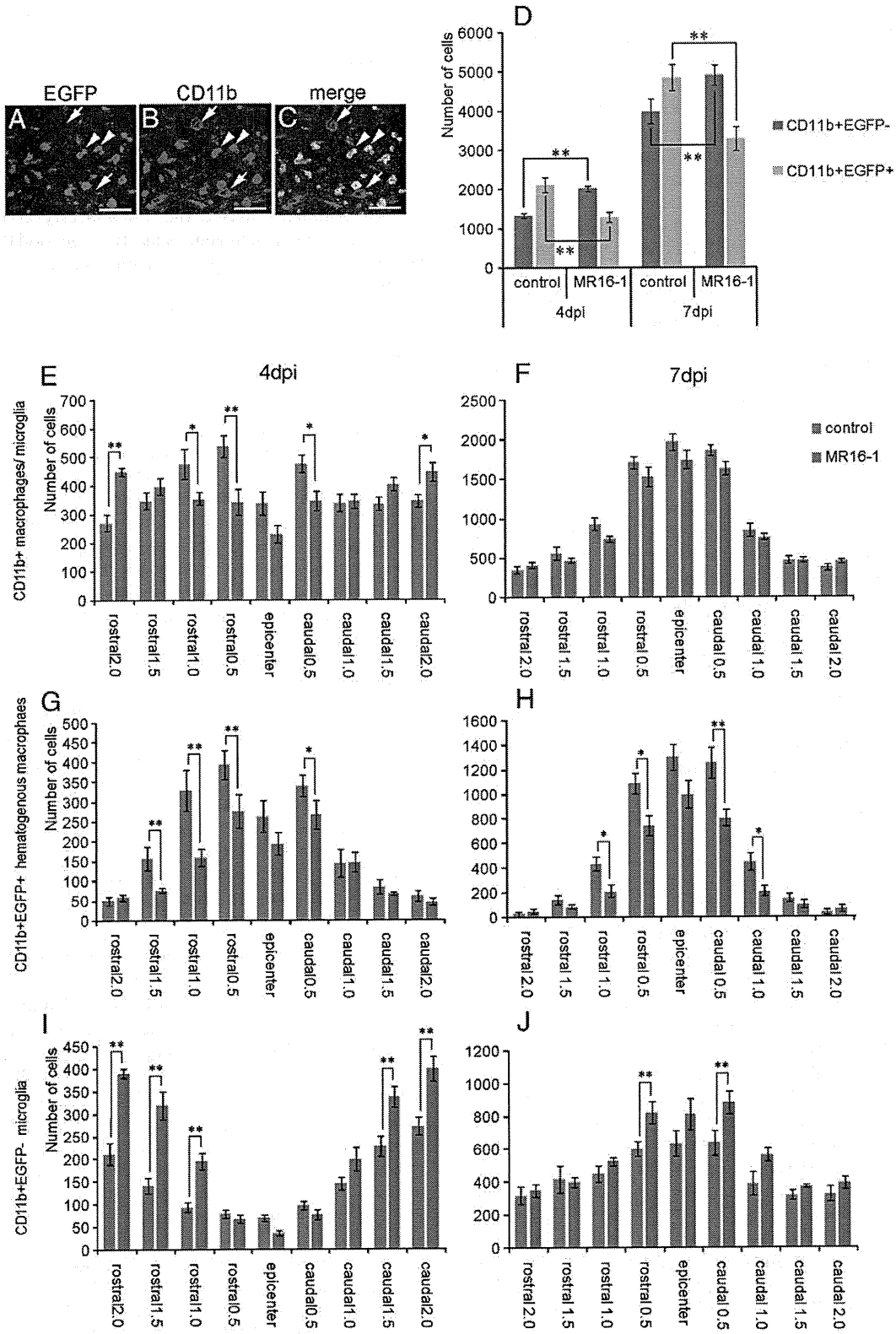

Fig. 2. MR16-1 treatment switches the major inflammatory cell type, from hematogenous macrophages to resident microglia. Analysis using chimeric mice. A–C: Immunostaining for EGFP (A, green) and CD11b (B, red), showing the distribution of $CD11b^+EGFP^+$ hematogenous macrophages (arrowheads) and $CD11b^+$ $EGFP^-$ resident microglia (arrows) in the injured spinal cord (C, merged). D: In the MR16-1-treated group, the major player in the inflammation switched from $CD11b^+EGFP^+$ hematogenous macrophages (light gray) to $CD11b^+EGFP^-$ resident microglia (dark gray) at 4 and 7 dpi. Number and distribution of macrophages/microglia in the spinal cord at 4 and 7 dpi. E, F: MR16-1 did not significantly affect the total number of inflammatory cells ($Cd11b^+$) at 4 (E) or 7 (F) dpi. G, H: MR16-1 reduced the recruitment of $CD11b^+EGFP^+$ hematogenous macrophages at 4 (G) and 7 (H) dpi. I, J: MR16-1 treatment increased the number of $CD11b^+EGFP^-$ resident microglia 1.0 to 2.0 mm rostral and caudal to the lesion epicenter at 4 dpi (I). At 7 dpi, both groups showed a shift in $CD11b^+EGFP^-$ microglia to the lesion epicenter, where the number of $CD11b^+EGFP^-$ microglia was significantly higher in the MR16-1-treated animals (J). Values are means ± SEM. $^*P<0.05$. $^{**}P<0.01$. Scale bars = 50 μm in A–C.